

AD-A246 044



2

NAVAL POSTGRADUATE SCHOOL

Monterey, California



DTIC
ELECTE
FEB 18 1992
S D

THESIS

FREE ELECTRON LASER
SHORT PULSE SIMULATION
AND TWO-MODE SIDEBAND ANALYSIS

by
Gregory A. Cord

June, 1991

Thesis Advisor:

W. B. Colson

Approved for public release; distribution is unlimited

92

92-03670



UNCLASSIFIED

SECURITY CLASSIFICATION OF THIS PAGE

REPORT DOCUMENTATION PAGE				
1a. REPORT SECURITY CLASSIFICATION Unclassified			1b. RESTRICTIVE MARKINGS	
2a. SECURITY CLASSIFICATION AUTHORITY			3. DISTRIBUTION/AVAILABILITY OF REPORT Approved for public release; distribution is unlimited.	
2b. DECLASSIFICATION/DOWNGRADING SCHEDULE				
4. PERFORMING ORGANIZATION REPORT NUMBER(S)			5. MONITORING ORGANIZATION REPORT NUMBER(S)	
6a. NAME OF PERFORMING ORGANIZATION Naval Postgraduate School	6b. OFFICE SYMBOL (If applicable) PH	7a. NAME OF MONITORING ORGANIZATION Naval Postgraduate School		
6c. ADDRESS (City, State, and ZIP Code) Monterey, CA 93943-5000		7b. ADDRESS (City, State, and ZIP Code) Monterey, CA 93943-5000		
8a. NAME OF FUNDING/SPONSORING ORGANIZATION	8b. OFFICE SYMBOL (If applicable)	9. PROCUREMENT INSTRUMENT IDENTIFICATION NUMBER		
8c. ADDRESS (City, State, and ZIP Code)		10. SOURCE OF FUNDING NUMBERS		
		Program Element No	Project No.	Task No
				Work Unit Accession Number
11. TITLE (Include Security Classification) FREE ELECTRON LASER SHORT PULSE SIMULATION AND TWO-MODE SIDEBAND ANALYSIS				
12. PERSONAL AUTHOR(S) GREGORY A. CORD				
13a. TYPE OF REPORT Master's Thesis	13b. TIME COVERED From To	14. DATE OF REPORT (year, month, day) JUNE 1991	15. PAGE COUNT 63	
16. SUPPLEMENTARY NOTATION The views expressed in this thesis are those of the author and do not reflect the official policy or position of the Department of Defense or the U.S. Government.				
17. COSATI CODES			18. SUBJECT TERMS (continue on reverse if necessary and identify by block number)	
FIELD	GROUP	SUBGROUP	FEL, Short pulse simulation, two-mode analysis, sidebands	
19. ABSTRACT (continue on reverse if necessary and identify by block number)				
<p>The Stanford Free Electron Laser (FEL), like many FELs is driven by extremely short electron pulses which drive equally short optical pulses. Simulations of the Stanford FEL describe the trapped-particle instability leading to sideband frequencies and limit-cycle behavior. Comparisons are made of recent experimental results that show close agreement between the desynchronism curves, optical spectra, and the electron spectra. The second part of this thesis analyzes sideband behavior when two modes are present in an FEL oscillator. Using two-mode wave and pendulum equations derived from maxwell's and the Lorentz force equations, the gain and phase shift for each initial phase of the two-mode optical field can be determined numerically. Averaging over all initial phases determines the FEL optical performance. In steady-state the presence of the sideband effectively reduces the undulators's length, delaying the onset of saturation. This allows more power to be generated in the optical field then possible with only a single mode.</p>				
20. DISTRIBUTION/AVAILABILITY OF ABSTRACT <input checked="" type="checkbox"/> UNCLASSIFIED/UNLIMITED <input type="checkbox"/> SAME AS REPORT <input type="checkbox"/> DTIC USERS			21. ABSTRACT SECURITY CLASSIFICATION Unclassified	
22a. NAME OF RESPONSIBLE INDIVIDUAL W. B. Colson			22b. TELEPHONE (Include Area code) (408) 646-2765	22c. OFFICE SYMBOL PH/Cw

DD FORM 1473, 84 MAR

83 APR edition may be used until exhausted
All other editions are obsoleteSECURITY CLASSIFICATION OF THIS PAGE
UNCLASSIFIED

Approved for public release: distribution is unlimited.

**FREE ELECTRON LASER SHORT PULSE SIMULATION
AND TWO-MODE SIDEBAND ANALYSIS**

by

G. A. Cord

Lieutenant, United States Navy

B. S., University of Arizona, 1982

Submitted in partial fulfillment of the
requirements for the degree of

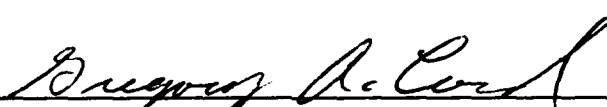
MASTER OF SCIENCE IN PHYSICS

from the

NAVAL POSTGRADUATE SCHOOL


June 1991

Author:



Gregory A. Cord


Approved by:



William B. Colson, Thesis Advisor



John R. Neighbours, Second Reader



Karlheinz E. Woehler, Chairman,
Department of Physics

ABSTRACT

The Stanford Free Electron Laser (FEL), like many FELs is driven by extremely short electron pulses which drive equally short optical pulses. Simulations of the Stanford FEL describe the trapped-particle instability leading to sideband frequencies and limit-cycle behavior. Comparisons are made of recent experimental results that show close agreement between the desynchronism curves, optical spectra, and the electron spectra.

The second part of this thesis analyzes sideband behavior when two modes are present in an FEL oscillator. Using two-mode wave and pendulum equations derived from Maxwell's and the Lorentz force equations, the gain and phase shift for each initial phase of the two-mode optical field can be determined numerically. Averaging over all initial phases determines the FEL optical performance. In steady-state the presence of the sideband effectively reduces the undulator's length, delaying the onset of saturation. This allows more power to be generated in the optical field than possible with only a single mode.

Accession For	
NTIS GRA&I	J
DTIC TAB	U
Unannounced	FI
Justification	
By	
Distribution	
Availability Codes	
Dist	Availability Codes
A-1	



Table of Contents

I. INTRODUCTION	1
II. FREE ELECTRON LASER THEORY	3
A. BASIC FREE ELECTRON LASER PHYSICS	3
B. THE SIMPLE PENDULUM EQUATION	5
C. THE SELF-CONSISTENT WAVE EQUATION	7
D. PHASE-SPACE AND THE LOW CURRENT, LOW GAIN FEL	9
E. SIDEBANDS AND THE TRAPPED-PARTICLE INSTABILITY	12
III. COMPARING SIMULATIONS AND EXPERIMENTAL OBSERVATIONS OF THE TRAPPED-PARTICLE INSTABILITY IN THE STANFORD FEL	15
A. INTRODUCTION	15
B. SHORT PULSE THEORY AND EFFECTS	16
C. SIMULATIONS AND EXPERIMENTAL OBSERVATIONS	19
D. CONCLUSION	26
IV. TWO-MODE THEORY AND SIDEBAND ANALYSIS	28
A. INTRODUCTION	28
B. TWO-MODE THEORY	29
C. TWO STEADY-STATE MODES	32
D. STEADY-STATE PHASE-SPACE EVOLUTION	35
E. TWO-MODE GAIN AND PHASE SHIFT	38
F. TWO-MODE SATURATION	49

G. CONCLUSION	54
LIST OF REFERENCES	55
INITIAL DISTRIBUTION LIST	56

ACKNOWLEDGEMENT

The author is grateful for support of this work by the Naval Postgraduate School, and the U. S. Office of Naval Research. The author would also like to thank W. B. Colson for his invaluable assistance.

I. INTRODUCTION

Free Electron Lasers (FELs) hold the promise of being reliable, versatile, and powerful sources of coherent radiation. The initial concept for the FEL was first proposed by John Madey in 1970 [Ref. 1]. He and his colleagues successfully demonstrated an operating FEL in 1976 and 1977 [Ref. 2,3]. Since then, many FELs have been built and are operating at Universities and Government Labs around the world, with still more projects on the drawing board. Active research continues in all aspects of FELs, from the basic physics of the FEL interaction to lasing with harmonics and ultra short-undulators.

There are many reasons for the interest shown in FEL design and operation. Using a relativistic electron beam as the source for coherent radiation the FEL has the potential for average optical power outputs in the multi-megawatt range. An FEL can be made continuously tunable over an order-of-magnitude by adjustments in the electron beam energy or the undulator magnetic field strength. Since the FEL interaction takes place in a vacuum containing nothing but electrons, a magnetic field, and light, the problems confronting high power lasers using some type of lasing medium are absent in the FEL.

Many of today's FELs use rf accelerators that produce extremely short electron pulses driving equally short optical pulses in an FEL oscillator. Because of their reliability and maturity, rf accelerators for the near future will continue to play an important role in FEL design. Short electron pulses and the non-linear trapped-particle instability combine to cause optical sidebands and limit-cycle behavior of the output power. Experiments run at the Stanford FEL which demonstrated these characteristics and are compared to simulations performed at the Naval Postgraduate School. Chapter II gives a brief overview of FEL theory while chapter III discusses the characteristics of short pulse FELs and analyzes the results from the Stanford FEL

experiment and simulations.

The formation of sidebands are not limited to short-pulse FELs. Any FEL with a strong enough optical field can generate a sideband from the electrons trapped in the optical field. Chapter IV uses a simple two-mode model to study sideband behavior. The electron motion in the presence of a sideband is analyzed, as well as the optical evolution of each mode. This research gives a better understanding of FEL performance with sidebands present.

The most significant contributions in this thesis are summarized below.

1. Short pulse simulations of the Stanford FEL qualitatively and quantitatively model results from experiments exhibiting the trapped-particle instability and limit cycle behavior.
2. The effect of the trapped-particle instability on the electron phase-space dynamics is explained.
3. The effect of individual sideband phases on electron dynamics and optical development is examined.
4. The mechanism by which sidebands act to decrease the undulator's effective length, leading to higher power at saturation, is explained.
5. The validity of the two-mode wave equations are verified over a wide range of conditions by comparisons with energy conservation methods.
6. The two-mode wave equations are used to analyze the gain for each mode separately, as well as the optical field phase shift.

II. FREE ELECTRON LASER THEORY

A. BASIC FREE ELECTRON LASER PHYSICS

An FEL consists of three major components, an electron accelerator, an undulator or wiggler consisting of a periodic magnetic field, and an optical resonator to store the amplified light in the case of an FEL oscillator. A relativistic beam of electrons enters the undulator causing them to "wobble" as they traverse its length. The wobbling electrons spontaneously radiate in a narrow cone in the forward direction. With mirrors placed on each end of the undulator, some of the radiation is stored. Subsequent electrons entering the undulator undergo stimulated emission in the presence of the stored radiation leading to coherent radiation.

The description above uses quantum mechanical concepts to describe the basic FEL interaction, but due to the large number of photons in the FEL resonator at any time, the optical field can be described as a classical electromagnetic wave [Ref. 4]. Therefore, classical electromagnetic theory can be used to describe the interaction between electrons, light, and the undulator. Figure 2-1 illustrates a relativistic electron inside an undulator being acted upon by the undulator field and a radiation or optical field. When the electron is given a velocity component out of the paper or in the y direction due to the undulator field and at the same time the magnetic field from the optical wave is directed downwards in the $-x$ direction, then, the electron experiences a retarding force opposing its forward motion down the axis of the undulator. This opposing Lorentz force causes the electron to lose energy. Since the interaction occurs in a vacuum, the energy loss from the electron goes to the optical field causing amplification. The phase of the electrons relative to the optical wave is extremely important. If a majority of electrons are in the wrong phase they will gain energy from

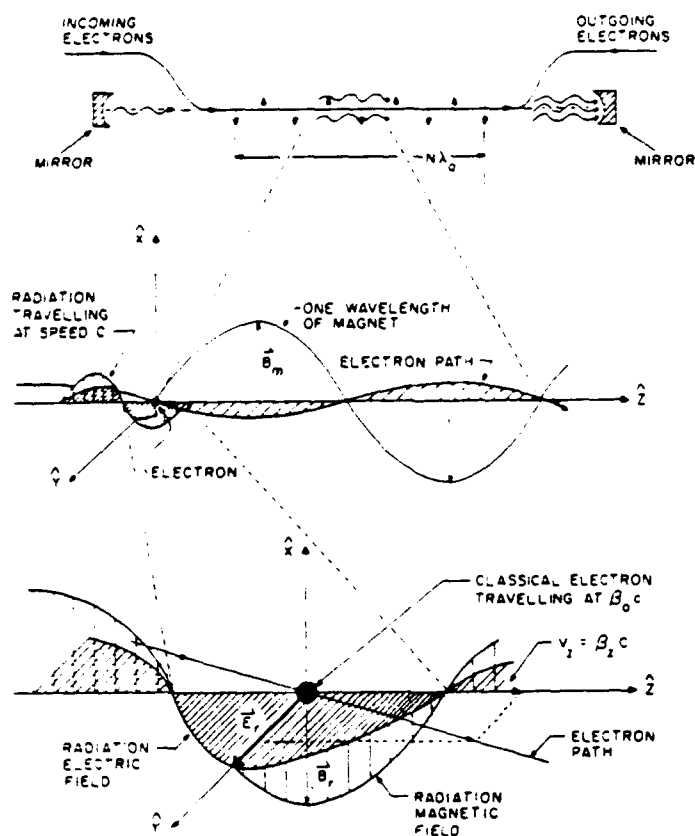


Figure 2-1: Electron motion inside an FEL undulator

the optical field. As will be shown, the electron dynamics and optical field development can be described with a simple pendulum equation and self-consistent wave equation.

Before going on further with a classical approach to FEL dynamics, it should be noted that one of the consequences of using relativistic electrons is the possibility of generating short wavelength light. Electrons entering the undulator with energy γmc^2 where γ is the Lorentz factor, m the electron mass, and c the velocity of light, will see the undulator wavelength λ_0 is Lorentz contracted. The relativistic electrons will radiate laser light with a wavelength $\lambda = \lambda_0/2\gamma^2$. By changing the electron beam energy, the laser can be continuously tuned to different wavelengths. A typical FEL

with $\lambda_0 = 5$ cm using a 50 MeV electron beam will radiate at $\lambda \approx 2\mu\text{m}$. A doubling of the electron beam energy causes the FEL to approach optical wavelengths.

B. THE SIMPLE PENDULUM EQUATION

In order to understand the FEL interaction it is first necessary to understand the individual electron motion in the presence of the optical and undulator fields as governed by the Lorentz force equations

$$\frac{d(\gamma\vec{\beta})}{dt} = \frac{-e}{mc} [\vec{E}_R + \vec{\beta} \times (\vec{B} + \vec{B}_R)] \quad , \quad (2-1)$$

$$\frac{d\gamma}{dt} = \frac{-e}{mc} \vec{\beta} \cdot \vec{E}_R \quad , \quad \gamma^2 = 1 - \vec{\beta} \cdot \vec{\beta} \quad ,$$

where \vec{E}_R and \vec{B}_R are the optical electric and magnetic fields, \vec{B} is the undulator magnetic field, $|e|$ is the electron charge magnitude, and $\vec{\beta}c$ is the electron velocity. It should be noted that this and all other derivations assume cgs units. For simplicity and for the sake of consistency with the rest of the thesis, the undulator is assumed to be helically polarized with a static magnetic field of the form

$$\vec{B} = B(\cos(k_0 z), \sin(k_0 z), 0) \quad , \quad (2-2)$$

where B is the magnetic field strength, $k_0 = 2\pi/\lambda_0$ is the undulator's field wave number, and z is the longitudinal distance along the undulator. The optical field present in the undulator is assumed to be a circularly polarized plane wave with the form

$$\vec{E}_R = E(\cos\psi, -\sin\psi, 0) \quad , \quad \vec{B}_R = E(\sin\psi, \cos\psi, 0) \quad , \quad (2-3)$$

where E is the optical field strength, and $\psi = kz - \omega t + \phi$ with k the wave number, ω the radial frequency, and ϕ the optical phase angle.

Substituting (2-2) and (2-3) into the Lorentz force equations (2-1) and separating the equations into components of transverse (perpendicular) motion, and longitudinal

(z-motion) yields

$$\frac{d(\gamma\vec{\beta}_\perp)}{dt} = \frac{-e}{mc} [E(1 - \beta_z)(\cos\psi, -\sin\psi, 0) + \beta_z B(-\sin k_0 z, \cos k_0 z, 0)] , \quad (2-4)$$

$$\frac{d(\gamma\beta_z)}{dt} = \frac{-e}{mc} [E(\beta_x \cos\psi - \beta_y \sin\psi) + B(\beta_x \sin k_0 z - \beta_y \cos k_0 z)] , \quad (2-5)$$

$$\frac{d\gamma}{dt} = \frac{-e}{mc} E[\beta_x \cos\psi - \beta_y \sin\psi] , \quad (2-6)$$

where $\vec{\beta}_\perp = (\beta_x, \beta_y, 0)$. For relativistic electrons $\beta_z \rightarrow 1$, so that $E(1 - \beta_z) \ll B\beta_z$, and transverse motion due to the optical field in (2-4) may be neglected. This allows (2-4) to be solved by inspection yielding the transverse electron motion

$$\vec{\beta}_\perp = -\frac{K}{\gamma} (\cos k_0 z, \sin k_0 z, 0) , \quad (2-7)$$

where $K = eB\lambda_0/2\pi mc^2$, and is referred to as the undulator parameter. For most FEL applications $K \approx 1$. approximation. Substituting (2-7) into (2-6) gives the electron energy change with respect to time

$$\dot{\gamma} = \frac{eKE}{\gamma mc} \cos(\zeta + \phi) , \quad (2-8)$$

where $\zeta = (k + k_0)z - \omega t$ is a dimensionless microscopic variable that describes the electrons phase with respect to the optical and undulator field. From (2-8), if $-\pi/2 < \zeta + \phi < \pi/2$, the electrons will be gaining energy from the optical wave, while if $\pi/2 < \zeta + \phi < 3\pi/2$, the electrons are losing energy to the optical wave. If electrons with an initial random dispersion in ζ can be made to bunch with $\pi/2 < \zeta < 3\pi/2$ as they travel down the undulator, then the FEL will experience growth of the optical wave.

Further simplification of (2-8) can be made by relating γ to $\ddot{\zeta}$. By noting that $\gamma^2 = 1 - \beta_z^2 - \beta_\perp^2$, it can be shown that [Ref. 4]

$$\lambda = \frac{\lambda_0(1 + K^2)}{2\gamma^2} \quad (2-9)$$

which is referred to as the resonance condition, and

$$\dot{\gamma} = \frac{\gamma \ddot{\zeta}}{2k_0 c} = \frac{\gamma \ddot{\zeta}}{2\omega_0} \quad (2-10)$$

Equating (2-8), the energy equation and (2-10) results in the simple pendulum equation

$$\ddot{\zeta} = \frac{2e\omega_0 KE}{\gamma 2mc} \cos(\zeta + \phi) \quad (2-11)$$

A more useful form of (2-11) is constructed by defining a dimensionless time $\tau = ct/L$. Note that $\tau = 0 \rightarrow 1$ as the electrons travel down the length of the undulator. The simple pendulum equation now becomes

$$\zeta^{\circ\circ} = |a| \cos(\zeta + \phi) \quad (2-12)$$

where " $\circ\circ$ " refers to differentiation with respect to τ , and the dimensionless optical field is $a = |a|e^{i\phi}$ where the dimensionless optical field strength is $|a| = (4\pi e K E L N)/(\gamma^2 m c^2)$. Since $|a|$ is proportional to the optical wave field strength E , it is indeed meaningful and (2-12) shows how the changes in electron phase and energy are dependent on the phase position and optical field strength. The next step is to derive an equation which expresses the change in the field a in terms of ζ .

C. THE SELF-CONSISTENT WAVE EQUATION

The Lorentz force equation was used to describe the electron dynamics within the optical and undulator fields. To describe the optical wave evolution requires the use of Maxwell's wave equation

$$\left[\nabla^2 - \frac{1}{c^2} \frac{\partial^2}{\partial t^2} \right] \vec{A} = -\frac{4\pi}{c} \vec{J}_\perp \quad (2-13)$$

where the vector potential for the optical field is given by

$$\vec{A} = \frac{E_R}{k}(\sin\psi, \cos\psi, 0) \quad , \quad (2-14)$$

and \vec{J}_\perp is the transverse current from the transverse electron beam motion. The optical field is taken to vary slowly over an optical wavelength ($\dot{E}_R \ll \omega E_R$, $\dot{\phi} \ll \omega \phi$). This is referred to as the slowly-varying-amplitude-and-phase-approximation (SVAP) which is to be expected from a coherent light source. This approximation allows second derivatives resulting from (2-13) to be neglected resulting in

$$\left[\nabla^2 - \frac{1}{c^2} \frac{\partial^2}{\partial t^2} \right] \vec{A} \approx \frac{2}{c} \frac{\partial E_R}{\partial t} (\cos\psi, -\sin\psi, 0) \quad (2-15)$$

$$- \frac{2E_R}{c} \frac{\partial \phi}{\partial t} (\sin\psi, \cos\psi, 0) = -\frac{4\pi}{c} \vec{J}_\perp \quad ,$$

from the substitution of (2-14) into (2-13).

Looking at the right hand side of (2-13), the electron current is given by $\vec{J}_\perp = -ec\vec{\beta}_\perp \delta^3(\vec{x} - \vec{r}_i)$ where \vec{r}_i is the position of the i 'th electron, and $\delta^3(\vec{x} - \vec{r}_i)$ is the three dimensional Dirac delta function [Ref. 5]. Substituting in the electron transverse motion β_\perp from (2-7) yields the transverse particle current

$$\vec{J}_{\perp i} = \frac{e^2 B}{\gamma m \omega_0} (\cos k_0 z, \sin k_0 z, 0) \delta^3(\vec{x} - \vec{r}_i) \quad . \quad (2-16)$$

Substituting (2-16) into (2-15), projecting two orthogonal unit vectors

$$\hat{\epsilon}_1 = (\cos\psi, -\sin\psi, 0) \quad \hat{\epsilon}_2 = (\sin\psi, \cos\psi, 0) \quad (2-17)$$

onto the resultant yields two equations. Summing over all particles to obtain the total transverse current, and averaging both equations at a fixed time over a small volume element [Ref. 3] gives

$$\frac{1}{c} \frac{\partial E_R}{\partial t} = -\frac{2\pi e K}{\gamma} \rho \langle \cos(\zeta + \phi) \rangle \quad , \quad (2-18)$$

and

$$E_R \frac{1}{c} \frac{\partial \phi}{\partial t} = -\frac{2\pi e K}{\gamma} \rho \langle \sin(\zeta + \phi) \rangle \quad , \quad (2-19)$$

where p is the electron particle density, and the brackets represent the average value taken from all the sampled electrons. By defining the dimensionless current density as

$$j = \frac{8N(e\pi KL)^2 p}{\gamma^3 mc^2} \quad , \quad (2-20)$$

equations (3-6) and (3-7) are further simplified to

$$|\dot{a}| = -j \langle \cos(\zeta + \phi) \rangle \quad , \quad (2-21)$$

and

$$\dot{\phi} = \frac{j}{|a|} \langle \sin(\zeta + \phi) \rangle \quad . \quad (2-22)$$

Equations (2-21) and (2-22) show how the optical wave amplitude and phase evolve with the electron phase ζ . Bunching of the electrons around the phase $\zeta = \pi$ leads to growth of the optical wave and gain, while bunching electrons around $\zeta = \pi/2$ causes the optical phase to be driven. Increasing the current density j can lead to high gain and large phase evolution, but as the optical field increases it will act as a retarding influence on the phase evolution. Values of $j \approx \pi$ result in low gain, while values of $j \gg \pi$ result in high gain.

D. PHASE SPACE AND THE LOW CURRENT, LOW GAIN FEL

The electron phase velocity is given by

$$v = \dot{\zeta} = L[(k_0 + k)\beta_z - k] \quad . \quad (2-23)$$

The phase velocity v increases with electron energy, and decreases when the electron loses energy to the optical wave. When $v = 0$, the electron is said to be at resonance with the undulator and optical fields. A resonant electron will pass through one undulator period as one optical wavelength passes over it. This condition, while giving maximum coupling with the optical field, does not give maximum gain for a collection of electrons that are initially dispersed in ζ along many optical wavelengths. The initial conditions of any electron in phase space are given by $\zeta_0 = \zeta(0)$ and $v_0 = v(0)$ at $\tau = 0$.

In the case of low gain or low j , the optical field experiences only small changes down the length of the undulator. For this case the electrons follow approximately fixed paths in phase-space as in the case of a simple pendulum. The fixed phase space paths are given by

$$v^2 = v_0^2 - 2|a|[\sin(\zeta + \phi) - \sin(\zeta_0)] \quad (2-24)$$

In the low gain regime, the phase-space points $v_0 = 0$ and $\zeta_0 = -3\pi/2, \pi/2$ are "unstable fixed points" that would correspond to a mechanical pendulum being at the top of its arc. Electrons near these points evolve slowly with time. The point $v_0 = 0$ and $\zeta_0 = \pi/2$ are "stable fixed points", corresponding to a pendulum at the bottom of its arc. Electrons at these points do not evolve at all. The "separatrix" is a curve in phase space that separates open and closed phase-space paths, and is given by

$$v_s^2 = 2|a|[1 - \sin(\zeta_s + \phi)] \quad (2-25)$$

which is derived by substituting the values for the unstable fixed points into (2-23). The peak-to-peak height of the separatrix is $4|a|^{1/2}$, and the horizontal position is determined by the optical phase ϕ .

Figure 2-2 illustrates electron evolution in the $(\zeta, v = \dot{\zeta})$ phase space for weak fields, $|a| \leq \pi$, and low gain, $j < \pi$, by numerically solving the pendulum and wave equations. The electrons are injected into the undulator at $\tau = 0$ with $j = 1$, at an initial energy slightly off resonance $v_0 = 2.6$, uniformly distributed in phase $\zeta_0 = -\pi/2 \rightarrow 3\pi/2$, into an optical field with an initial value of $|a(0)| = a_0 = \pi$. As the electrons evolve in τ , they become darker, and are finally black at $\tau = 1$. The separatrix is drawn defining the boundary between closed and open phase-space paths. From the initial positioning, some of the electrons gain energy from the optical field and move ahead of the average flow of electrons. Other electrons lose energy to the optical field and slip behind the flow in phase. The combination of the two causes phase bunching near $\zeta \approx \pi$ at $\tau = 1$. From (2-21) as stated previously, bunching near this phase causes gain in the optical wave. Another way to view this is that the net electron

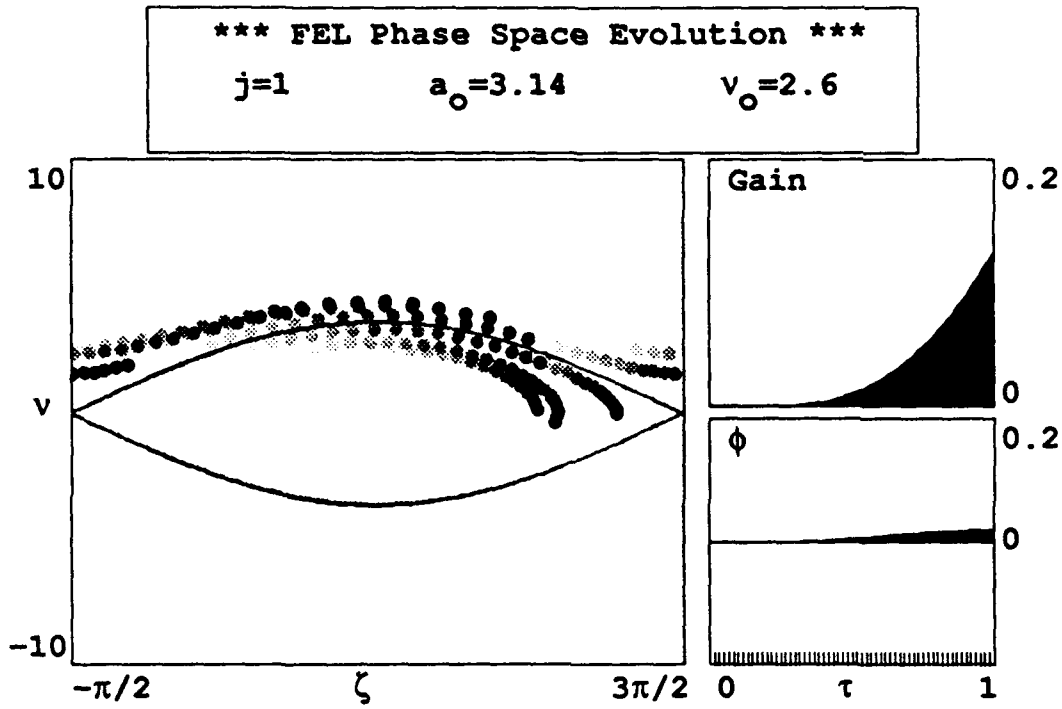


Figure 2-2: Electron phase space evolution in weak fields

energy has decreased from $\tau=0 \rightarrow 1$ because $\langle v(\tau=1) \rangle$ is less than $\langle v(\tau=0) \rangle$. Plotted to the right in figure 2-2 is the gain in optical energy $G(\tau) = (a(\tau)^2 - a_0^2)/a_0^2$, and the change in optical phase $\phi(\tau)$. Both the optical phase and amplitude start to be driven as the electrons begin to bunch.

For weak fields with low gain, the gain $G(\tau)$ can be solved analytically [Ref. 3] as well as numerically as demonstrated above. By assuming low gain and low current, the pendulum equation can be solved by perturbation theory to the lowest order in a_0 and j . By using energy conservation and assuming the electrons are initially uniformly distributed in phase ζ_0 and are monoenergetic with phase velocity v_0 , the average energy lost from an electron is $\gamma mc^2(\langle v \rangle - v_0)/4\pi N$. Substituting in the

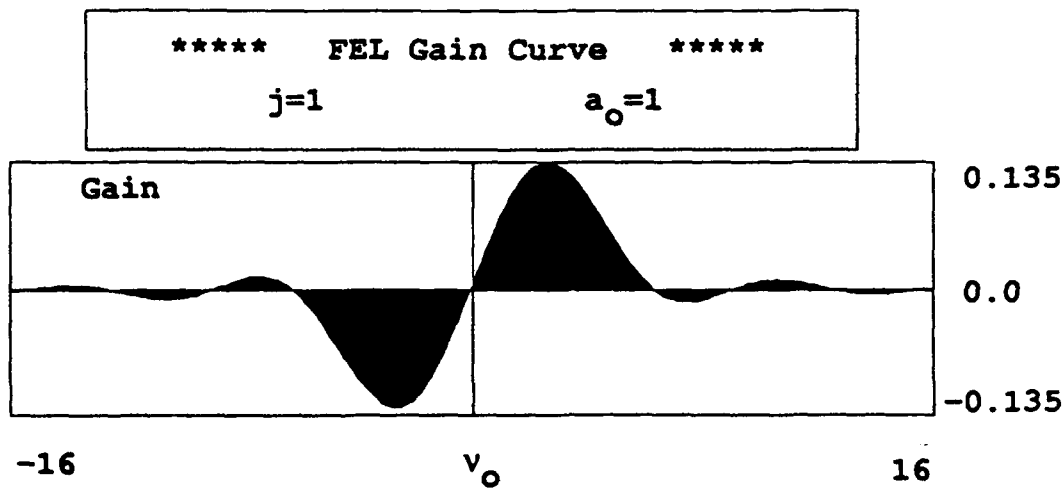


Figure 2-3: Gain spectrum for weak fields and low current

pendulum equation expansion results for $\langle v \rangle$ gives the small signal gain equation

$$G(\tau) = j \left[\frac{2 - 2\cos(v_0\tau) - v_0\tau \sin(v_0\tau)}{v_0^3} \right] \quad (2-26)$$

Figure 2-3 plots the optical field gain at $\tau = 1$ as a function of initial electron phase velocity v_0 . The curve is anti-symmetric about $v_0 = 0$ and has a maximum at $v_0 = 2.6$. The maximum small-signal gain is given by $G = 0.135j$ at $v_0 = 2.6$. The implications of the gain curve are that electrons at resonance, $v_0 = 0$, while having the maximum coupling with the optical wave will lose as much energy as they gain while electrons slightly off resonance drive the optical field amplitude.

E. SIDEBANDS AND THE TRAPPED-PARTICLE INSTABILITY

In strong optical fields, the electrons can be trapped in deep potential wells formed by the combined optical and undulator field forces. Electrons near the bottom of the well oscillate in harmonic orbits at the synchrotron frequency. As mentioned previously $\zeta \approx \pi/2 - \phi$ is a fixed point in phase space of ζ vs. $v = \dot{\zeta}$. By taking $\zeta' = \pi/2 + x$ and expanding the simple pendulum equation (2-12) in x for $x \ll \pi/2$ it

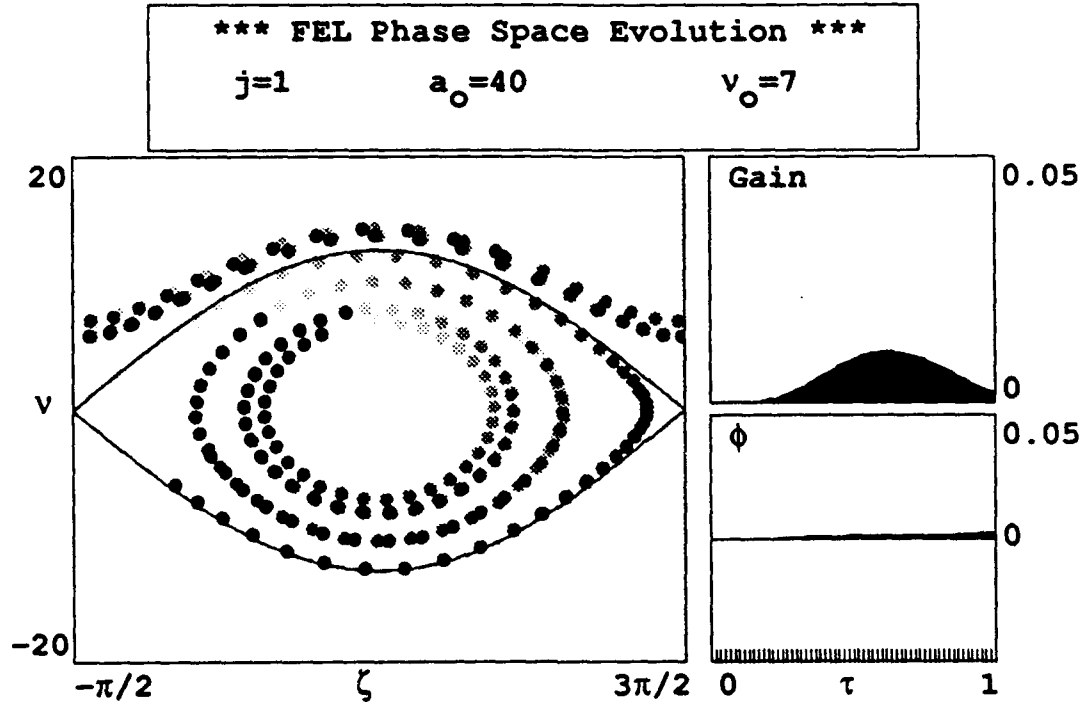


Figure 2-4: Phase space illustration of trapped-particle instability

can be seen that electrons close to the fixed point will oscillate with a synchrotron frequency of $v_s = |a|^{1/2}$. For an electron to complete one full synchrotron oscillation requires $|a|^{1/2} = 2\pi$, or $|a| = 4\pi^2 = 40$. This corresponds to a peak-to-peak separatrix height of $4|a|^{1/2} = 25$. Figure 2-4. shows a phase-space evolution of 10 sample electrons evolving from $\tau = 0 \rightarrow 1$. The electrons are initially evenly distributed in ζ , and are given the same initial phase velocity v . With an optical field strength of $a = 40$, dimensionless particle density of $j = 1$, and an initial optical phase $\phi = 0$, the electrons closest to the stable point $\zeta = \pi/2$ complete one full synchrotron oscillation.

As the electrons slip back past the optical wave due to the difference in relative speeds, the electrons continue to execute synchrotron oscillations which modulate the

optical wave. The modulations appear as sidebands centered around the fundamental frequency ν_0 by a difference of ν_s . In the case of one synchrotron oscillation or single sideband, the sideband spacing from the fundamental mode is given by $\nu_s = 2\pi$. For multiple sidebands the spacing from the fundamental is $\nu_s \approx 2\pi n$, where $n = 1, 2, 3, \dots$. It should be noted that the shift in wavelength from the fundamental wavelength is given by $\Delta\lambda/\lambda = \nu_s/2\pi N$.

In an FEL oscillator where the sideband is developed over many passes by the optical wave, the trapped-particle instability and sideband growth is dependent on the dimensionless current j and the loss factor for each pass Q . If J and Q are low enough the trapped-particle instability will not occur, and the FEL will produce a single mode. Sufficiently raising either j or Q however, will lead to the trapped-particle instability.

III. COMPARING SIMULATIONS AND EXPERIMENTAL OBSERVATIONS OF THE TRAPPED-PARTICLE INSTABILITY IN THE STANFORD FEL

A. INTRODUCTION

Short electron pulse FELs, such as the Stanford FEL have the unique ability to exhibit exotic non-linear effects in the optical field with only minor adjustments to the resonator mirrors. This characteristic allows differing FEL regimes to be studied without alterations to the initial electron beam entering the undulator.

Comparisons are made between experimental observations at the Stanford FEL and simulations run at the Naval Postgraduate School. Close agreement is found between the desynchronism curves, optical spectra, and the electron spectrum. Stable sideband development due to the trapped-particle instability is observed at Stanford, and predicted by simulations for the corresponding desynchronism value. At small desynchronism values, unstable sidebands are seen at Stanford as well as being predicted by simulation along with limit-cycle behavior.

The Stanford FEL [Ref. 6], like many FEL oscillators, is driven by short, picosecond electron pulses which drive equally short optical pulses. The Stanford Superconducting Accelerator (SCA) produces approximately 30,000 electron micropulses in each macropulse. Each micropulse is approximately 3 picoseconds long with an 84 nanosecond spacing between micropulses. The macropulse containing these short pulses has a length of three milliseconds with a 100 millisecond spacing between each macropulse. The spacing between macropulses ensures that any optical pulse in the FEL oscillator cavity will have decayed away prior to the following macropulse entering the undulator. The average macropulse current is $I \approx 200$ microamps and the initial electron beam energy is adjusted to alter the

wavelength of the emitted light between $\lambda = 3.7\mu\text{m}$ and $\lambda = 1.5\mu\text{m}$. The Stanford undulator consists of stationary magnets placed with $N = 120$ periods and a wavelength of $\lambda_0 = 3.6\text{cm}$. The peak magnetic field on axis is $B = 2900$ Gauss, giving an undulator parameter of $K \approx 0.7$.

B. SHORT PULSE THEORY AND EFFECTS

The method of determining the optical pulse evolution is based on the self-consistent numerical solution of the coupled Maxwell-Lorentz equations for the optical wave and electrons as discussed in section II, but with a few additions that deserve explanation [Ref. 7]. All longitudinal lengths with respect to the undulator, electron, and optical pulse are normalized by the slippage distance, $N\lambda$, so $Z/N\lambda \rightarrow z$. The slippage distance is the distance a resonant electron lags a point in the optical wave at the end of the undulator. Figure 3-1 illustrates the concept of slippage distance as the electron traverses one period of the undulator. The optical and electron pulse are divided up into equally spaced sites in z . The optical sites form spatial modes $a(z)$ which can be extended to equivalent longitudinal wavenumbers $a(k)$. The pendulum and wave equations (2-21,2-22) become slightly modified for pulse analysis with

$$\zeta_{z-\tau}^{\circ} = |a_z| \cos(\zeta_{z-\tau} + \phi_z) \quad , \quad (3-1)$$

and

$$\dot{a}_z^{\circ} = -j_{z-\tau} \langle \exp[i\zeta_{z-\tau}] \rangle \quad . \quad (3-2)$$

The subscript z denotes the position of an optical site in the undulator. The subscript $z-\tau$ denotes the corresponding electron site that was previously ahead of the optical site along the length of the undulator. The need for two separate subscripts arises due to the difference in velocity between the optical pulse and the electron pulse. The light traveling at speed c , remains fixed in z , while the slower electrons slip back to site $z-\tau$. When the electrons pass through the undulator, those at a site z interact with a range of sites in the optical wave envelope. As the electrons slip back past the

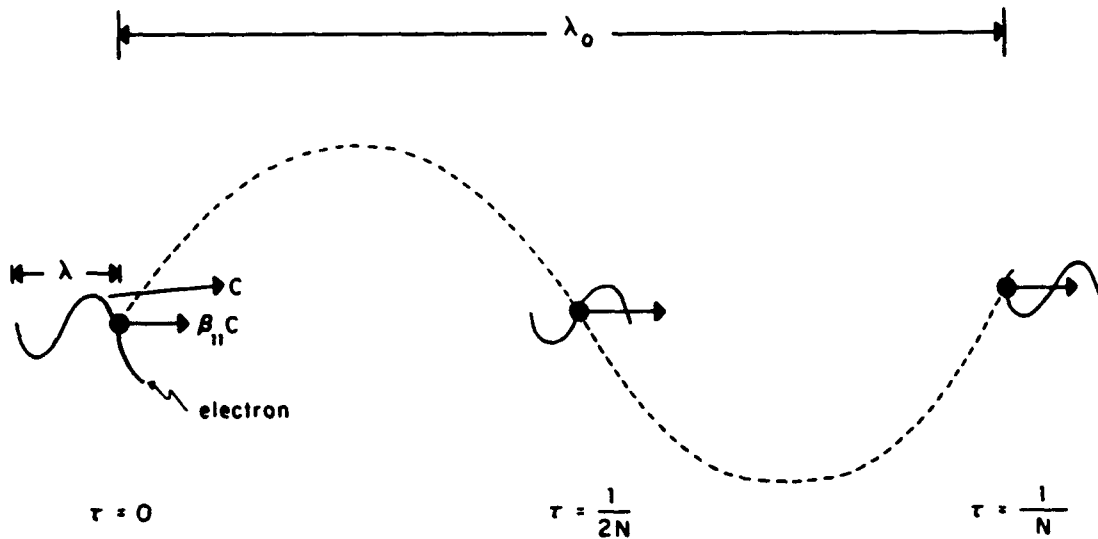


Figure 3-1: An electron traveling from left to right slips one optical wavelength λ as it traverses one undulator period λ_0

optical wave the electron beam and optical wave exchange information, and the electrons pass information from one optical field site to another. The dimensionless particle density is $j(z) = 8N(\pi eKL)^2 \rho(z)/\gamma^3 mc^2$, where $\rho(z)$ is the actual particle density at site z .

The electron pulse is assumed to have a parabolic profile given by $j = j_0(1 - 2z^2/\sigma_z^2)$ where σ_z is the electron pulse length and j_0 is the peak current. The electron pulse is represented by equally spaced electron sites that each hold an equal number of sample electrons. Like the electron pulse, the optical pulse is represented by sites the same distance apart as the electron sites. With each time-

step, as an optical site passes over an electron site, the pendulum and wave equation are numerically solved for the corresponding electron and optical interaction at each site.

In strong optical fields the electrons can be trapped in deep potential wells formed by the combined optical and undulator field forces. Electrons near the bottom of the well oscillate in harmonic orbits at the synchrotron frequency. By looking at the phase-space evolution of the electrons, it is observed that a field strength of $|a| = 4\pi^2$ causes one oscillation of the trapped electrons near the stable phase $\zeta = \pi/2$. The synchrotron frequency is given by $\nu_s = |a|^{1/2}$. The oscillation of the bunched electrons couples to the optical wave causing the amplitude and phase to oscillate at the synchrotron frequency leading to the formation of side-bands. The growth of the sideband power is the trapped-particle instability. The trapped-particle instability along with the extremely short longitudinal length of both the optical and electron pulse lead to exotic behavior that does not occur in FELs with longer pulses.

In a short-pulse FEL [Ref. 3,8], the optical pulse travels down the undulator at velocity c , while the electron pulse travels slightly slower at velocity $\beta_0 c$. The slippage distance $N\lambda$ measures the amount the electron pulse lags the optical pulse at $\tau = 1$. In an FEL oscillator, the electrons must be timed to enter the undulator each time the optical pulse makes one round trip $\Delta t = 2S/c$ where S is the mirror separation. Assuming the electron and optical pulses start out at the same time, the leading edge of the optical pulse will immediately start over-taking the electron pulse before any significant bunching of the leading electrons occurs. This lack of coupling between the initial edge of the optical pulse and the electrons causes the leading edge of the optical pulse to decay with time while building up the back of the optical pulse. The net result is that the optical pulse centroid has a speed slightly less than c . To account for this slower speed, the mirrors are placed slightly closer together than would be needed to synchronize an uncoupled pulse. The shorter distance is referred to as the desynchronism d , and normalized by the slippage distance $N\lambda$. The output

power and optical mode of an FEL are sensitive to slight variations in d . When d is too large, the electron and optical pulses do not overlap over a sufficient number of passes, and steady state FEL coupling can not be achieved. Decreasing d causes the coupling, and the optical power to increase. As d continues to decrease, the optical amplitude of the wave continues to increase leading to the trapped-particle instability and development of stable sidebands. Letting d get even smaller leads to even larger optical powers, and unstable sidebands that may be cyclic or chaotic over time. Near $d=0$, the optical power peaks, and then quickly goes to zero because the optical wave and electron pulse are again uncoupled.

For short-pulse FEL's the interaction at the edges of both the optical and electron pulse play a large part in determining the final optical power and waveform, along with helping to explain the sensitivity of the FEL to minor changes in d . This concept is best illustrated using parameters from the Stanford FEL. A 3.0 picosecond micropulse equates to a length of approximately $900\mu\text{m}$. When the FEL is lasing at $\lambda = 3.7\mu\text{m}$, the micropulse is only two slippage distances long. Since one electron site can exchange information along one slippage length within the optical wave and vice versa, the electrons that interact with the edge of the optical wave account for close to half of the total electrons in the beam. If the electron beam is made of longer pulses which cover many slippage distances, the edge effects of the electron beam and optical wave play a less significant role in the final optical output of the FEL.

C. SIMULATIONS AND EXPERIMENTAL OBSERVATIONS

A comparison between the observed [Ref. 9] and simulated desynchronism curve while lasing at $\lambda = 3.7\mu\text{m}$ is shown in figure 3-2. Both curves are quantitatively similar showing a peak power at $1\mu\text{m}$ desynchronism, corresponding to dimensionless desynchronism $\sigma \approx .002$. The optical power increases as d decreases. As d decreases, the FEL exhibits stable and unstable sideband operation. In the simulations, the distance z is given in terms of the slippage distance. The optical

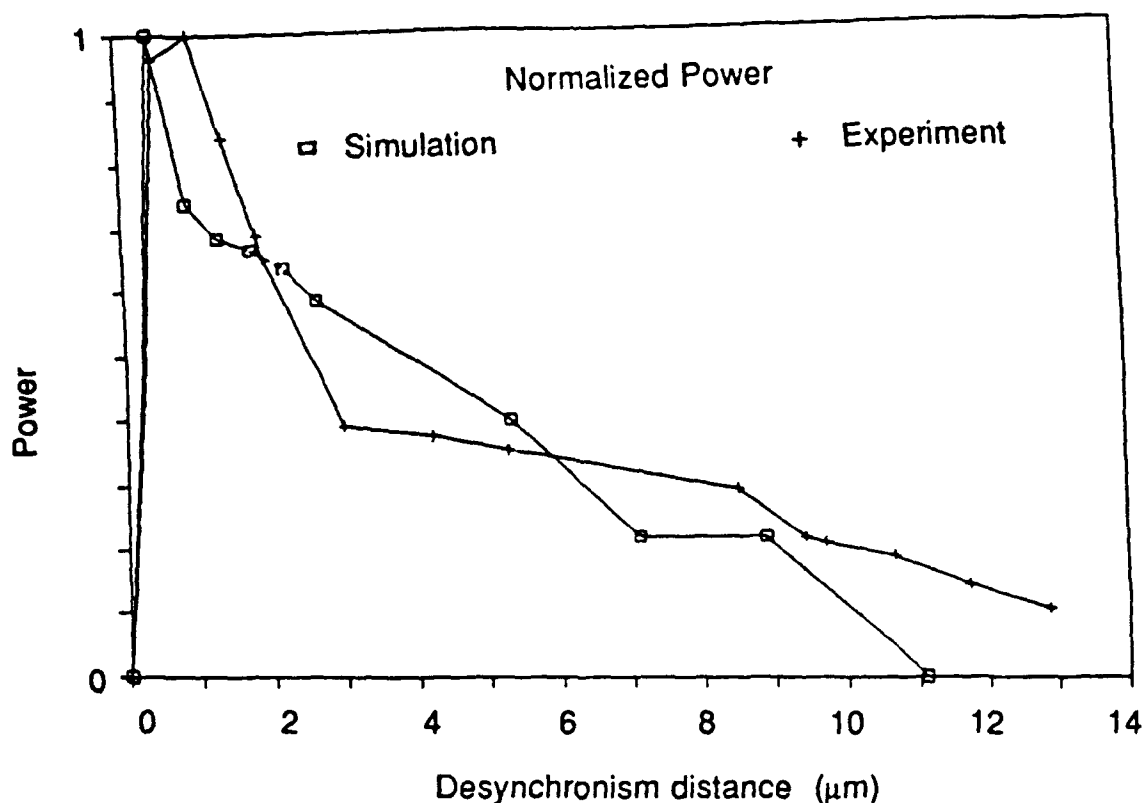


Figure 3-2: Simulation and experimental desynchronism curves at $\lambda = 3.7\mu\text{m}$ wavelength

power spectrum, $\log(P(v))$, and electron energy spectrum, $f(v)$, are given in terms of the dimensionless phase velocity $v = L[(k + k_0)\beta_z - k]$. The input parameters for the simulations are the particle density $j_0 = 0.5$, the electron pulse width in terms of the slippage distance $\sigma_z = 2.0$, the loss coefficient for each pass $Q = 140$, and the number of undulator periods $N = 120$.

The first comparison is made at a relatively large desynchronism $d = 0.018$. Figure 3-3 shows the simulation and experimental results for lasing at $\lambda \approx 3.7\mu\text{m}$ with a non-normalized desynchronism of $8\mu\text{m}$. From left to right, the three upper frames show the final pulse shape, optical spectrum, and electron spectrum at the end of the

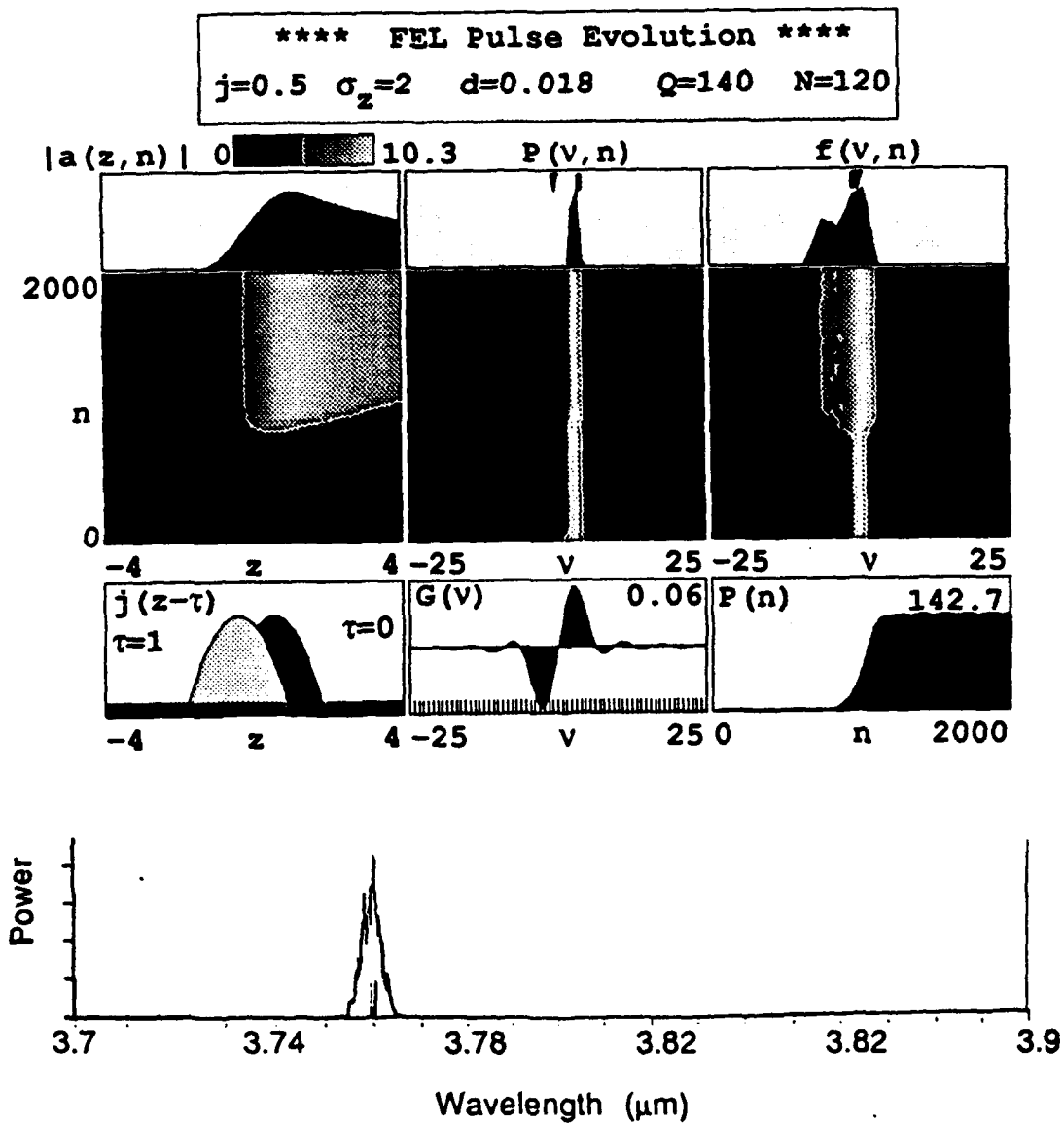


Figure 3-3: Simulation results and experimental power spectrum at $\lambda = 3.7\mu\text{m}$ wavelength, and with a desynchronism of $8\mu\text{m}$

simulation. The middle three frames, from left to right show the evolution of the optical pulse shape, optical spectrum, and electron energy spectrum versus the undulator pass number n . The lower three frames of the simulation display the electron pulse shape along with slippage, the small-signal gain spectrum $G(\nu)$, and the optical power P versus the undulator pass number n . The experimental power spectrum [Ref. 9] is presented below and plotted versus the optical wavelength λ . In the experiment, the optical power is time-averaged over many micropulses. The upper-center plot of the simulation shows the optical power spectrum $P(\nu)$ centered about the frequency for maximum small-signal gain. The experimental results show only a single optical frequency with no sidebands. Both experiment and simulation show weak optical fields with no trapped-particle instability, as demonstrated by no sidebands being present. The simulation has a maximum field of $|a(z)| = 10$ which is less than the required $\nu_s^2 = |a| \approx 4\pi^2$ for one synchrotron oscillation, and sideband development [Ref. 10]. The electron spectrum starts to spread out in the negative ν direction at $n \approx 800$ passes. This corresponds to the point where the optical and electron pulse start to reach strong fields and produce a steady state power level. The spreading out of the electron spectrum is due to electrons losing and gaining energy with respect to the optical wave.

Decreasing the desynchronism to $d = 0.003$ gives rise to the trapped-particle instability and sidebands. Figure 3-4 shows the results of lasing at $\lambda = 3.7\mu\text{m}$ and a desynchronism of $1.5\mu\text{m}$. The simulation shows that the optical field reaches $|a| \approx 40$, and is large enough to cause one synchrotron oscillation. The center-left frame in the simulation demonstrates how the optical pulse changes shape in a cyclic manner over time. The optical power spectrum is shown in the upper-center frame. This also illustrates the importance of the electron interaction between the leading and trailing edges of the optical wave. The center frame shows the growth of a stable sideband spaced $\nu_s \approx 5.0$ away from the fundamental. It should be noted that the fundamental is slightly to the right of maximum small-signal gain because of strong field saturation

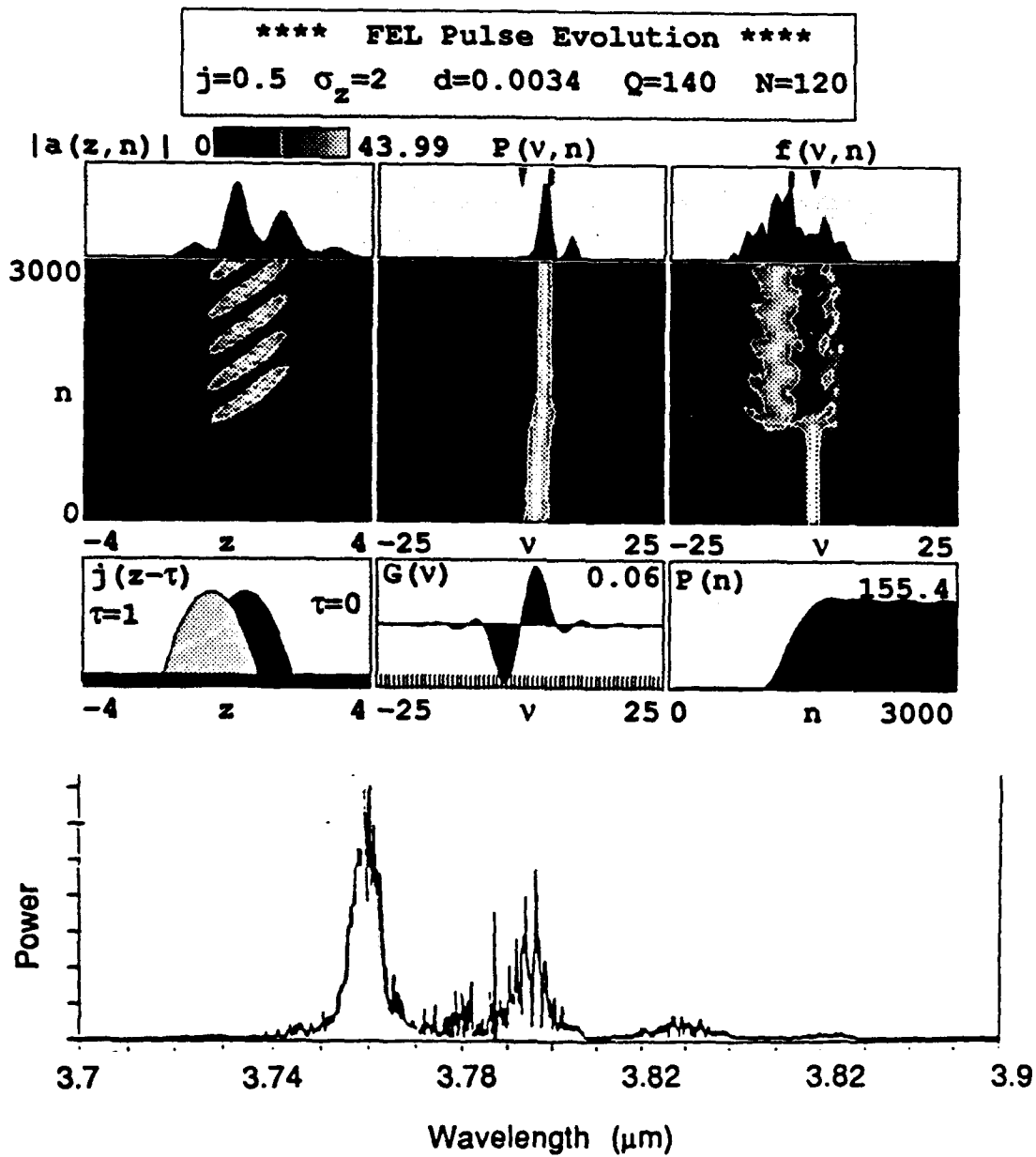


Figure 3-4: Simulation results and experimental power spectrum at
 $\lambda = 3.7\mu\text{m}$ wavelength, and with a desynchronism of $1.5\mu\text{m}$

[Ref. 4]. This shows good correlation with the observed experimental spectra shown below the simulation. Using $\nu_s \approx 2\pi N \Delta\lambda / \lambda$ we see that the sideband is spaced at $\nu_s \approx 7.0$ for the experimental observations. By comparing the right-bottom frames of the simulations in figure 3-3 and figure 3-4, it can be seen that the steady-state final optical power is greater with sidebands present. The formation of a sideband allows the FEL to obtain a higher optical power due to limiting the onset of saturation by effectively decreasing the length of the undulator. This is explained in greater detail in chapter 4.

Unstable sidebands occur as the desynchronism is further decreased to $d = 0.001$. Figure 3-5 shows lasing at $\lambda = 3.7\mu\text{m}$ with less than $0.5\mu\text{m}$ desynchronism in the Stanford experiment. Like the previous figure, the optical pulse changes its spatial shape in a cyclic manner over time. However, in this case $\nu_s^2 = |a| \approx 71$. The center frame shows that the sidebands are no longer steady, but are cycling in and out from the fundamental. In the simulation, this sideband evolution leads to limit-cycle behavior in the power. The bottom-right frame of the simulation shows how the optical power cycles around a steady-state value at the same frequency as the sideband oscillations. The experimental spectrum taken at the same value of d appears to be chaotic over time with no clear sideband structure at all. However, it should be noted that the experimental data was time-averaged over many hundreds of micropulses. It is quite possible that cyclic sidebands and limit-cycle behavior were present, but the spectral signature for this behavior was washed out in the time-averaging process. In either case, both simulation and observation show a broader optical spectrum than the previous examples along with increased optical power. From the simulation, it should be noted that the final electron spectrum is much more spread out than in the previous examples. This is again attributed to the increase in optical power as the electrons lose more energy per pass.

If the desynchronism is decreased to $d = 0.0$, so there is no desynchronism, the electron beam and optical field will not couple to produce gain and steady-state output.

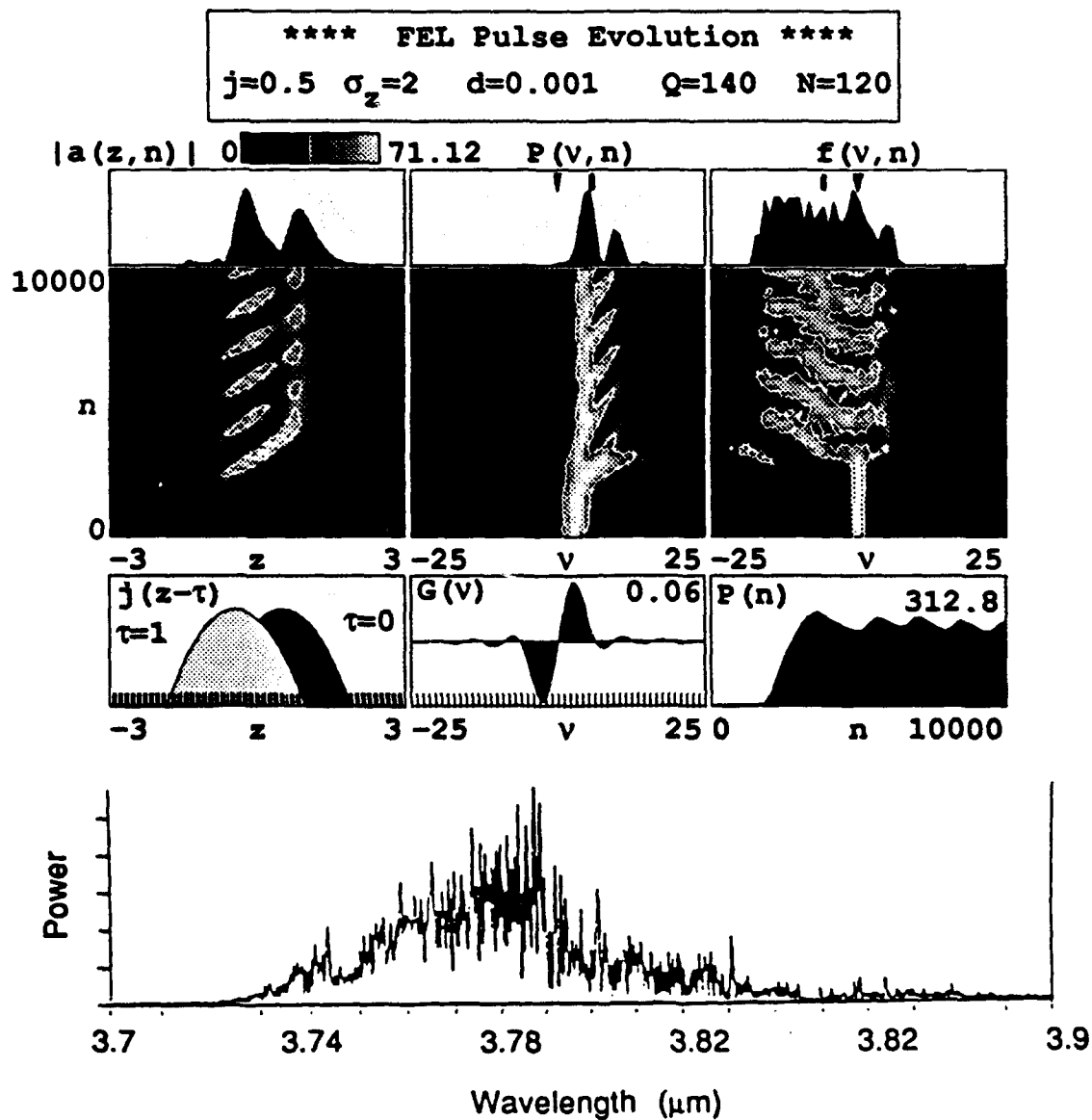


Figure 3-5: Simulation results and experimental power spectrum at $\lambda = 3.7\mu\text{m}$ wavelength, and with a desynchronism of $< 0.5\mu\text{m}$

Figure 3-6 is a simulation performed with $d = 0.0$. As can be seen, any growth of the optical wave and optical power is small and transient due to the lack of effective coupling between the optical pulse and the electron pulse.

The electron spectrum at the end of the undulator is also compared to experiments. Figure 3-7 shows the observed and simulated electron distribution after lasing at $\lambda = 1.5\mu\text{m}$ with a stable optical pulse that exhibits no sidebands. The energy spread is given in terms of the electron phase velocity v where $\Delta v \approx 4\pi N \Delta E / E$, and ΔE is the spread in electron energy away from E . For the experimental observation, the curve centered at $\Delta E = 0$ is the electron energy spread prior to the FEL interaction for the experiment. The frame at the right shows the electron energy spread after the FEL interaction in the simulation. The width of the energy spread is proportional to the optical power, $\Delta v \approx 4|a|^{1/2}$. In the simulation the spread is $\Delta v \approx 16$, and in the experiment the spread is $\Delta v \approx 13$. Both experiment the simulation show two distinct peaks, these can be most easily explained by phase-space bunching of the electrons at an energy close to resonance and at an energy less than resonance.

D. CONCLUSION

From the comparisons done above, it is clear there that there is close agreement between the desynchronism curves, optical spectra, and the electron spectrum. The simulations qualitatively model the Stanford experiments throughout a range of desynchronism values, including those in which exotic short-pulse effects are demonstrated. Stable and unstable sidebands due to the trapped-particle instability are experimentally observed, and predicted by simulations at corresponding desynchronism values. While limit-cycle behavior, predicted by simulation, is not positively confirmed by experimental results, the chaotic optical spectra observed at small desynchronism is an indication that limit-cycle behavior may actually be occurring in the Stanford FEL.

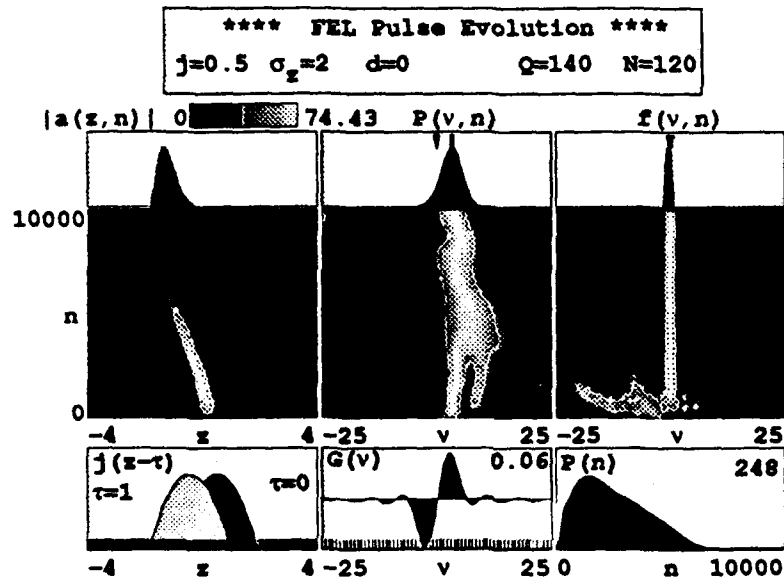


Figure 3-6: Simulation results at $\lambda = 3.7\mu\text{m}$ wavelength, and with a desynchronism of $0.0\mu\text{m}$

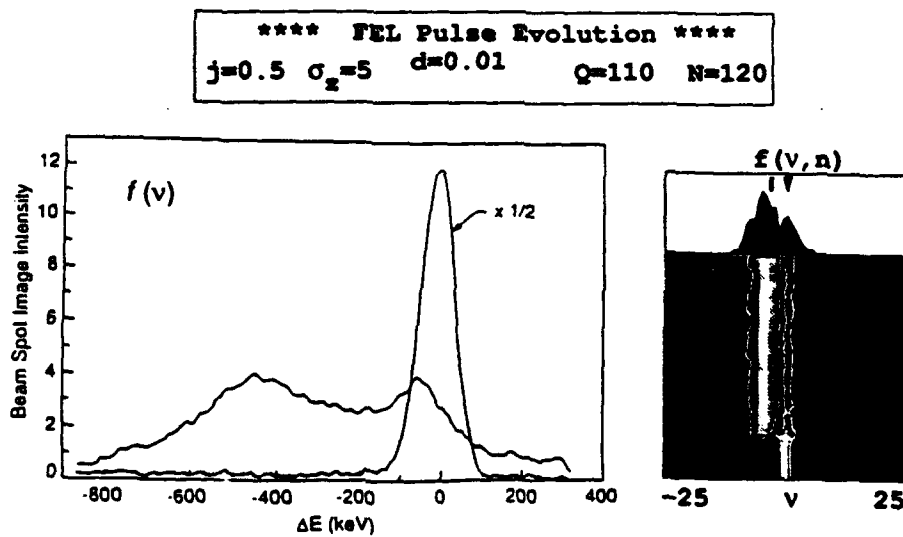


Figure 3-7: Simulation and experimental electron spectra at $\lambda = 1.5\mu\text{m}$ wavelength for a stable optical pulse

IV. TWO MODE THEORY AND SIDEBAND ANALYSIS

A. INTRODUCTION

In an FEL oscillator with strong optical fields, the electrons can be trapped in deep potential wells formed by the combined optical and undulator field forces. Electrons near the bottom of the well oscillate in harmonic orbits at the synchrotron frequency. The electron motion causes a modulation in the optical field which can be amplified into a sideband after multiple passes of the optical wave through the undulator. This process is referred to as the trapped-particle instability as discussed in section II.

The trapped-particle instability and subsequent sideband development are strong non-linear effects that have important consequences for present and future FEL operations. For many applications including weapons, the ideal FEL would have high optical power, narrow spectrum, and no sidebands. However, in the untapered FEL high power tends to cause the formation of sidebands, and the more sidebands present the higher the power and the greater the FEL efficiency. By decreasing the resonator Q , or the beam current j the sideband power can be decreased or completely suppressed. However, this comes at the expense of degraded FEL performance. As mentioned in the previous chapter, short pulse FELs can control sideband power by mirror positioning, but once again this comes at the expense of FEL performance. Other methods for suppressing sidebands include selective resonators that impose a large loss on the optical field at or near the sideband frequencies. This too, limits FEL performance since the fundamental mode is limited in growth by its saturation mechanism.

To gain a better understanding of sideband development and operation, the FEL dynamics between electrons and optical field will be investigated for the situation where only two optical modes are allowed to exist. Allowing for two modes, a fundamental and lower sideband, simplifies the analysis over multiple sidebands while

still being representative of the conditions present in many FELs operating with sidebands.

B. TWO MODE THEORY

To study the electron and optical dynamics in the oscillator with two optical modes, equations of motion for the electrons must be developed and then used to derive the driving current in the optical wave equation. This can be accomplished in a manner similar to the single mode pendulum and wave equations [Ref. 11,12], producing a two-mode pendulum and wave equations.

With two optical modes present, the electron equations of motion are

$$\frac{d(\gamma\vec{\beta})}{dt} = -\frac{e}{mc}(\vec{E} + \vec{E}_s + \vec{\beta} \times (\vec{B}_m + \vec{B} + \vec{B}_s)) , \quad (4-1)$$

$$\frac{d\gamma}{dt} = -\frac{e}{mc}\vec{\beta} \cdot (\vec{E} + \vec{E}_s) , \quad (4-2)$$

where \vec{E} and \vec{B} are the electric and magnetic fields of the fundamental optical field, and \vec{E}_s and \vec{B}_s are the electric and magnetic fields due to the sideband optical field. The undulator has a magnetic field denoted by \vec{B}_m . The fundamental and sideband optical fields are of the form

$$\vec{E} = E(\cos\psi, -\sin\psi, 0) , \quad \vec{B} = E(\sin\psi, \cos\psi, 0) , \quad (4-3)$$

$$\vec{E}_s = E_s(\cos\psi_s, -\sin\psi_s, 0) , \quad \vec{B}_s = E_s(\sin\psi_s, \cos\psi_s, 0) , \quad (4-4)$$

where $\psi = kz - \omega t + \phi$ and $\psi_s = k_s z - \omega_s t + \phi_s$, k and k_s are the wave numbers, ω and ω_s are the frequencies, and ϕ and ϕ_s are the phases of the respective waves. The undulator field is considered to be helical with a magnetic field of the form

$$\vec{B}_m = B(\cos(k_0 z), \sin(k_0 z), 0) . \quad (4-5)$$

Substituting (4-3),(4-4),(4-5) into the force equations (4-1),(4-2) and solving for the perpendicular electron motion while noting that the transverse force due the optical fields is negligible compared to the undulator field yields

$$\vec{\beta}_\perp = -\frac{K}{\gamma}(\cos(k_0 z), \sin(k_0 z), 0) \quad , \quad (4-6)$$

where $K = eB\lambda_0/2\pi mc^2$ is the undulator parameter. Eq. (3) now becomes

$$\frac{d\gamma}{dt} = \frac{e}{mc} \frac{K}{\gamma} (E \cos(k_0 z + \psi) + E_s \cos(k_0 z + \psi_s)) \quad . \quad (4-7)$$

Noting that $\gamma^2 = 1 - \beta_\perp^2 - \beta_z^2$, and using β_\perp in (8), this yields

$$\dot{\beta}_z = \frac{(1 + K^2)}{\gamma^2} \frac{\dot{\gamma}}{\gamma} \quad . \quad (4-8)$$

Defining $\zeta = (k + k_0)z - \omega t$ as the electron phase with respect to the fundamental optical wave, taking $d^2\zeta/dt^2$ along with the resonance condition $\lambda_0/2\lambda = \gamma^2/(1 + K^2)$, and equating $\dot{\beta}_z$ in terms of ζ and γ gives

$$\dot{\gamma} = \frac{\ddot{\zeta}}{(k + k_0)c} \frac{k}{2k_0} \approx \frac{\ddot{\zeta}}{2k_0 c} \quad , \quad (4-9)$$

since $k_0 \ll k$. Equating (4-7) and (4-9) while introducing the dimensionless time τ and the dimensionless optical fields $|a|$ and $|a_s|$ results in the two-mode pendulum equation

$$\overset{\circ}{v} = \overset{\circ}{\zeta} = |a| \cos(\zeta + \phi) + |a_s| \cos(k_0 z + \psi_s) \quad , \quad (4-10)$$

where " $\overset{\circ}{}$ " denotes $d/d\tau$. By using the approximation $k, k_s \gg k_0$ and the definition $\Delta v_s = ((k - k_s)/k)2\pi N$, the z dependence can be eliminated and the pendulum equation can be expressed as

$$\overset{\circ}{\zeta} = |a| \cos(\zeta + \phi) + |a_s| \cos(\zeta + \Delta v_s \tau + \phi_s) \quad . \quad (4-11)$$

As stated earlier, we are concerned with the first sideband caused by synchrotron oscillations occurring at $\Delta v = 2\pi$.

The next step is to develop a wave equation for the optical field. The two-mode optical field has the vector potential

$$\vec{A} = \frac{E}{k}(\sin\psi, \cos\psi, 0) + \frac{E_s}{k_s}(\sin\psi_s, \cos\psi_s, 0) \quad . \quad (4-12)$$

Substituting this into the general wave equation

$$\left[\nabla^2 - \frac{1}{c^2} \frac{\partial^2}{\partial t^2} \right] \vec{A} = -\frac{4\pi}{c} \vec{J}_\perp \quad (4-13)$$

where \vec{J}_\perp is the transverse current from the transverse motion of the electron beam, and applying the slowly varying amplitude and phase approximations to eliminate all terms with two derivatives, yields the left hand side of the wave equation.

$$\begin{aligned} \left[\nabla^2 - \frac{1}{c^2} \frac{\partial^2}{\partial t^2} \right] \vec{A} = & \frac{2}{c} \dot{E}(\cos\psi, -\sin\psi, 0) - \frac{2}{c} E \dot{\phi}(\sin\psi, \cos\psi, 0) \\ & + \frac{2}{c} \dot{E}_s(\cos\psi_s, -\sin\psi_s, 0) - \frac{2}{c} E_s \dot{\phi}_s(\sin\psi_s, \cos\psi_s, 0) \end{aligned} \quad (4-14)$$

As with the single mode wave equation [Ref. 5], the rapidly rotating terms of (4-14) are removed by projecting four polarization vectors onto the wave equation, and the right hand side of (4-13) is expressed in terms of the summation of single particle currents. Combining constants into dimensionless form results in the two-mode dimensionless wave equations

$$\begin{aligned} \dot{\hat{a}} + \dot{\hat{a}}_s \exp(i\Delta v_s \tau) &= -j \langle \exp(-i\zeta) \rangle \\ \dot{\hat{a}} + \dot{\hat{a}}_s \exp(i\Delta v_s \tau) &= -j \langle \exp(-i(1 - \Delta v_s/2\pi N)\zeta) \rangle \end{aligned} \quad (4-15)$$

By assuming that $\Delta v_s \ll 2\pi N$, consistent with the slow-varying amplitude and phase assumption, the two equations above are equivalent and the two-mode wave equation is just

$$\dot{\hat{a}} + \dot{\hat{a}}_s \exp(i\Delta v_s \tau) = -j \langle \exp(-i\zeta) \rangle \quad (4-16)$$

By assuming the gain for both the fundamental and sideband optical modes are small over one pass $\dot{\hat{a}}$ and $\dot{\hat{a}}_s$ can be separated allowing an equation for each mode. Integrating (4-16) over τ from 0 to 1 and letting $\Delta v_s \approx 2\pi$ results in

$$\Delta a = -j \langle \int_0^1 \exp(-i\zeta) d\tau \rangle \quad (4-17)$$

Multiplying (4-16) by $\exp(-i(\zeta + 2\pi\tau))$ and again integrating over time yields

$$\Delta a_s = -j \int_0^1 \exp(-i\zeta + 2\pi\tau) d\tau > \quad (4-18)$$

C. TWO STEADY-STATE MODES

Experimental data and full multi-mode simulations show that with one sideband present, it is not uncommon for a single sideband to have slightly less or as much power as the fundamental in steady-state. With this in mind, the case where both modes have the same optical amplitude and low gain will be looked at to illustrate the interaction between electrons and optical modes.

From an electron's frame of reference, as it travels down the undulator starting at $\tau = 0$, it will see N periods from the fundamental mode overtake it by the time it reaches the end of undulator at $\tau = 1$. If a sideband is present, offset from the fundamental by $\nu_s = 2\pi$, the electron will see $N-1$ sideband periods overtake it as well. If both modes are pictured as rotating polarization vectors, the sideband vector will rotate once, or 2π relative to the fundamental mode vector as the electron passes down the undulator. This will cause interference of the optical field dependent on τ . In essence, the electrons feel the force from a beat wave composed of two different amplitudes and frequencies. The total optical field experienced by an electron at any time, $|a_t(\tau)|$, is the sum of the fundamental and sideband optical field at τ . If the sideband polarization vector is assumed to rotate relative to a fixed fundamental vector with a frequency of $2\pi\tau$, the total dimensionless optical field strength is given by

$$|a_t(\tau)| = [|a|^2 + |a_s|^2 + 2|a||a_s|\cos(2\pi\tau + \phi_s)]^{1/2} \quad (4-19)$$

where ϕ_s is the initial phase angle of the sideband, with the fundamental assumed to have an initial phase angle of zero. From (4-19) it can be seen for given values of $|a|$ and $|a_s|$, the maximum and minimum values for the total optical field strengths are independent of the initial phase difference ϕ_s . However, the value of τ at which the maximum and minimum occur is dependent on the initial values of ϕ_s . The value of ϕ_s has an important influence on the electron dynamics and optical gain.

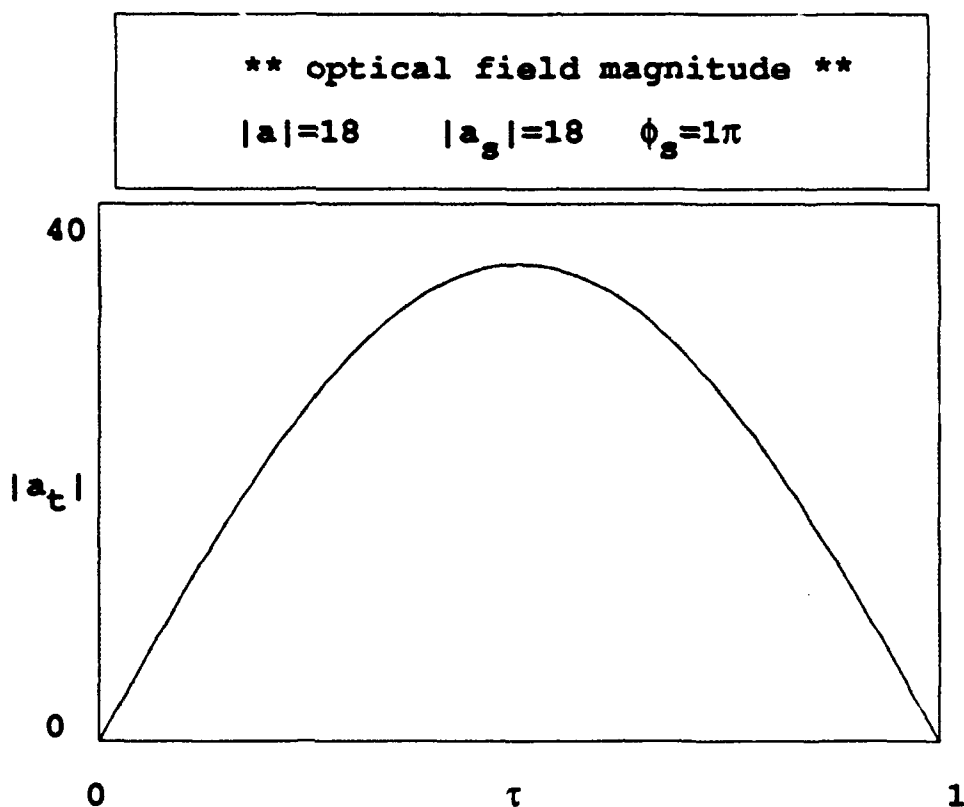


Figure 4-1: Optical field profile experienced by an electron with $\phi_s = \pi$

Figure 4-1 plots the total optical field experienced by the electrons versus τ , with $|a| = |a_s| = 18$, and $\phi_s = \pi$. Electrons injected into an undulator containing this field would experience the maximum force due to the optical electric field at $\tau = 0.5$ and a minimum of zero force at $\tau = 0$ and $\tau = 1.0$. Compare this with figure 4-2, where $|a|$ and $|a_s|$ are the same but $\phi_s = 0.4\pi$. The maximum and minimum amplitudes are the same, as figure 4-1, but the field is offset by $\tau = 0.3$. The optical field profiles in figures 4-1 and 4-2 not only represent the field strength with respect to τ as experienced by a relativistic electron, but can also be thought of as the shape of the optical wave that overtakes an electron traveling down the undulator. The parabolic shape shown in both figures represents one slippage distance length of the optical

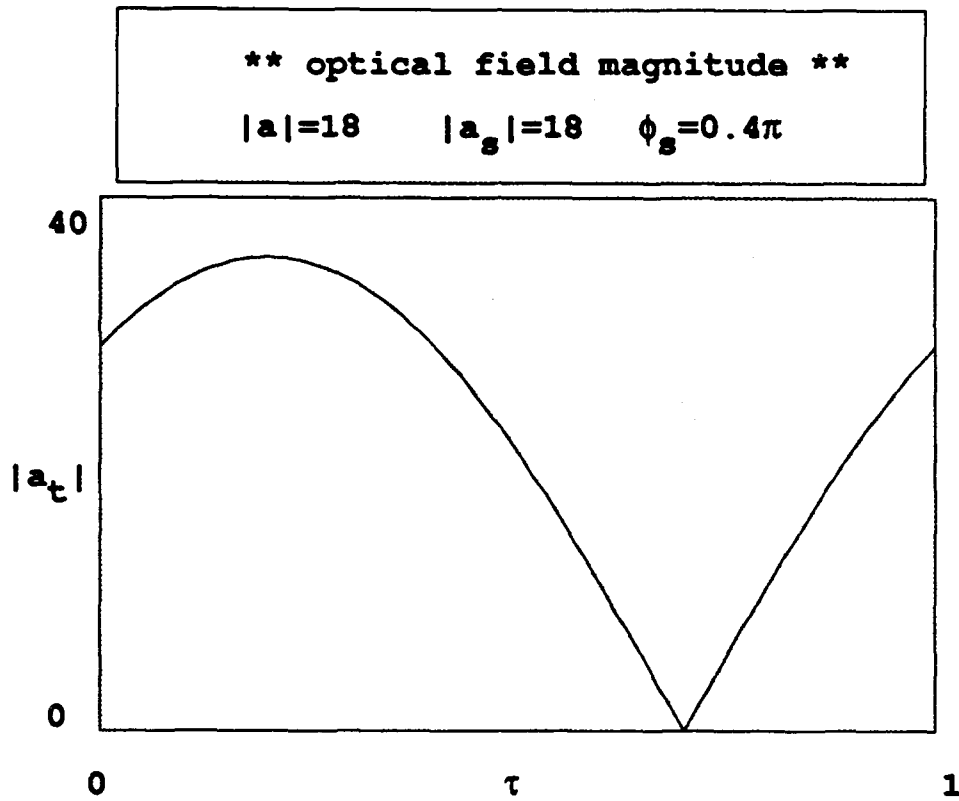


Figure 4-2: Optical field profile experienced by an electron with $\phi_s = 0.4\pi$

field, only inverted. This means that the field strength shown at $\tau = 0$ is the leading edge of the optical envelope, and the field strength shown at $\tau = 1$ is the trailing edge, referring to the end of a slippage distance. The optical wave itself is made up of a continuous series of parabolic-shaped fields which is nothing more than the absolute value of the Fourier transform of a two mode frequency spectrum of equal magnitude. An electron traveling down the undulator will only see one slippage distance of the optical field. Different electrons start at different positions within the slippage distance corresponding to different values of ϕ_s . For an electron beam with a long pulse, length $\gg N\lambda$, all values of ϕ_s are sampled equally. For an electron beam with a short pulse, length $< N\lambda$, values of ϕ_s are not sampled equally. Another consequence of

the optical field profiles shown in figures 4-1 and 4-2 is that the effective length of the undulator is shortened. At the points of the undulator where the optical field strength is close to zero, the undulator acts like a drift space where the electrons feel no phase-space forces. This will prove important when the saturation mechanisms for the two-mode FEL are compared to a single-mode FEL later in this chapter.

D. STEADY-STATE PHASE-SPACE EVOLUTION

The above section discussed the optical field present in an FEL oscillator at steady-state with a single sideband of equal magnitude to the fundamental present. The next step is to see what effect this field has on the electron beam. By numerically solving the two-mode pendulum equation (4-11) for low gain, figure 4-3 shows the phase-space evolution of 8 sample electrons as τ goes from $0 \rightarrow 1$. The electrons are lightly shaded at $\tau = 0$, gradually getting darker as $\tau \rightarrow 1$. The electrons sampled are uniformly distributed over a single wavelength λ of the fundamental and cover electron phases $\zeta = 0 \rightarrow 2\pi$. Other parts of the beam several wavelengths ahead and behind start at a different phase ϕ_s . The initial phase velocity is $v_0 = 2.6$ which is chosen for consistency with weak field models, but does not necessarily give the highest gain in stronger fields with sidebands present. The initial conditions are the same as used to develop the optical field profile in figure 4-1. The electron phase-space motion shown in figure 4-3 is caused by the changing optical field in figure 4-1. A better understanding of the electron motion can be realized using the two-mode pendulum equation written as

$$\ddot{\zeta} = |a_f(\tau)| \cos(\zeta) \quad , \quad (4-20)$$

where $|a_f(\tau)|$ is defined by (4-19). Equation (4-20) is analogous to the single-mode pendulum equation (2-12), except the dimensionless optical amplitude is changing with τ . With this in mind, the electron phase-space paths shown in figure 4-3 are easily explained. At $\tau = 0$ the electrons sense little or no optical field and just drift in phase-space with constant phase velocity v_0 . As τ increases so does the optical field until it

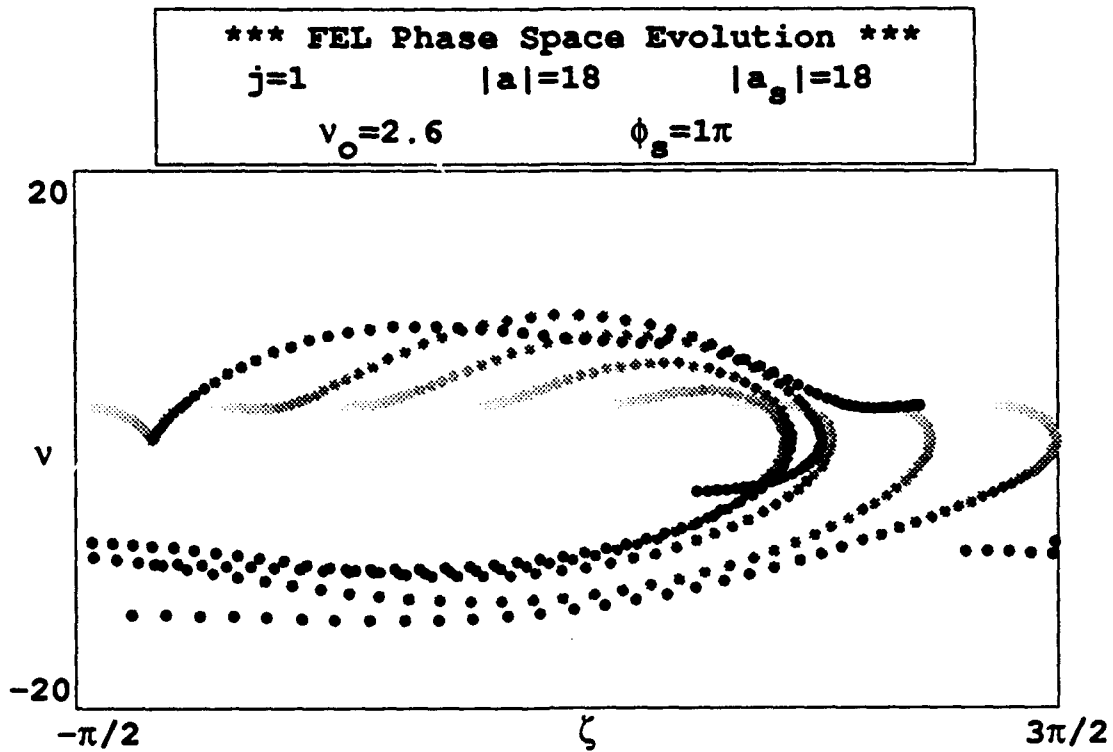


Figure 4-3: Phase-space evolution of sample electrons with $\phi_s = \pi$

peaks at $\tau = 0.5$. While the optical field is increasing the electrons are being driven into curved phase-space paths with the majority of electrons decreasing in phase velocity or losing energy. After the optical field peaks it decreases to zero as $\tau \rightarrow 1$. As the field strength decreases only electrons close to resonance, $v = 0$, will continue to be effected by the optical field. The majority of electrons, with $v < 0$, will start to drift in phase-space open orbits as demonstrated by the lower darkened electrons in the figure. For single-mode phase-space evolution, a separatrix was defined as the phase-space path dividing open orbits from closed orbits for all τ . For the two-mode pendulum equation a true separatrix does not exist because the optical field strength is constantly changing with τ . It is helpful to look at an "instantaneous separatrix", a

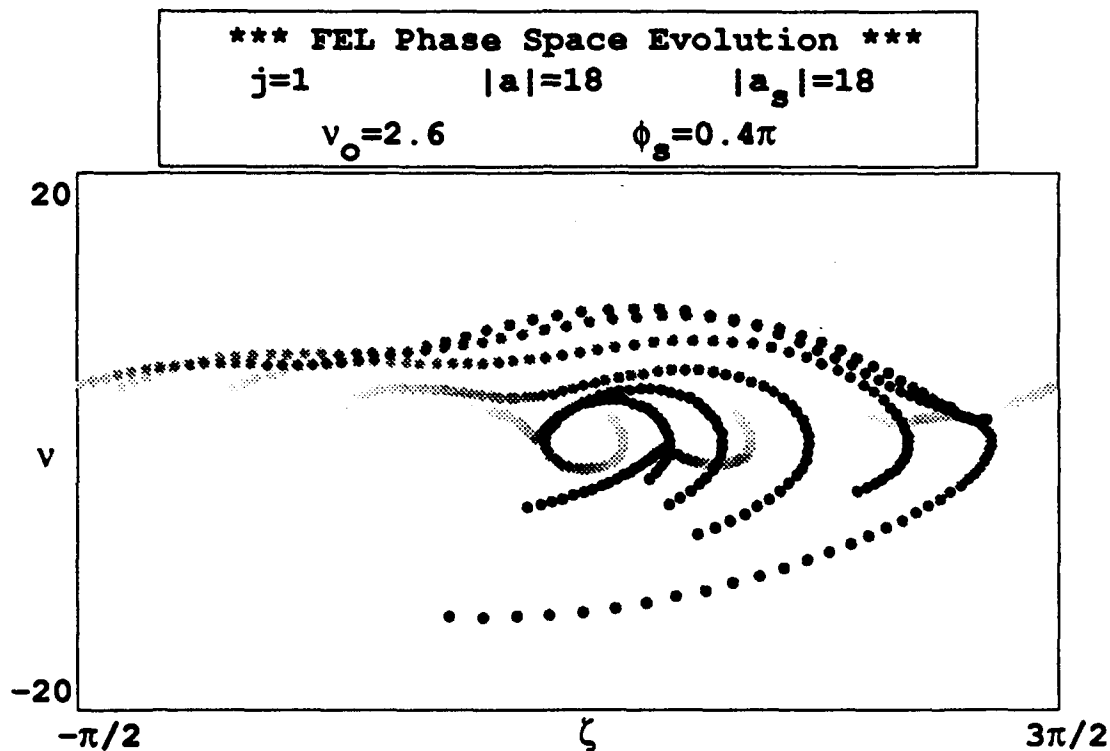


Figure 4-4: Phase-space evolution of sample electrons with $\phi_s = 0.4\pi$

separatrix defined at each instant τ . This instantaneous separatrix will grow and shrink in amplitude as the optical field strength increases and decreases with τ . When the separatrix reaches its maximum height all the electrons are captured in closed orbits. As the separatrix decreases in amplitude, electrons further off resonance will start going into open orbits. This again explains the phase-space paths demonstrated in figure 4-3. It turns out that $\phi_s \approx \pi$ is the initial sideband phase that generates the most gain.

Figure 4-4 shows the phase-space evolution with the same initial parameters as figure 4-3 with the exception that $\phi_s = 0.4\pi$, which corresponds to the optical field profile of figure 4-2. It is clearly evident that changing the initial phase difference

between fundamental and sideband has a dramatic effect on the electron phase-space paths. Unlike the previous example, the optical field $|a_r|$ starts close to a maximum at $\tau \approx 0$. This causes electrons distributed in ζ between $\pi/2$ and π to experience the greatest change in phase velocity v , a consequence of (4-20). As the optical field starts to decrease the separatrix shrinks, some electrons are placed in open orbits while others take on less severely curved phase-space paths. Once the field reaches a minimum and starts to increase, electrons that were previously in open orbits have now drifted into phases that experience the greatest phase acceleration. These electrons are deaccelerated to lower values of v as demonstrated by the darkened electrons on the right side of the figure.

E. TWO-MODE GAIN AND PHASE SHIFT

Once the electron phase-space trajectories are understood, the next step is to investigate the effects of the electron motion on the optical wave for the case of low gain. Assuming the electrons entering the undulator are uniformly distributed in the microscopic phase ζ_0 , and monoenergetic with phase velocity v_0 , the average energy lost by an electron is $\gamma mc^2(\langle v \rangle - v_0)/4\pi N$, and the gain of the optical field can be expressed as $G = 2j(v_0 - \langle v \rangle)/a_0^2$ [Ref. 4]. This allows the gain to be calculated from the phase-space plots with nothing more than the two-mode pendulum equation and the low gain assumption that $|a|$ and $|a_s|$ do not change enough from $\tau = 0 \rightarrow 1$ to effect the electron phase-space evolution. Calculating the gain in this manner uses energy conservation between electrons and optical field.

Figure 4-5 is a plot of gain versus initial sideband phase ϕ_s . Like the previous examples, $|a| = |a_s| = 18$, $j=1$, and $v_0 = 2.6$. The gain, $G(\phi_s)$, is a maximum at a sideband phase of $\phi_s = \pi$, and the gain averaged over all initial sideband phases is $G = 0.02$. As expected from the phase-space plots of different initial phase angles, the gain is dependent on the initial sideband phase.

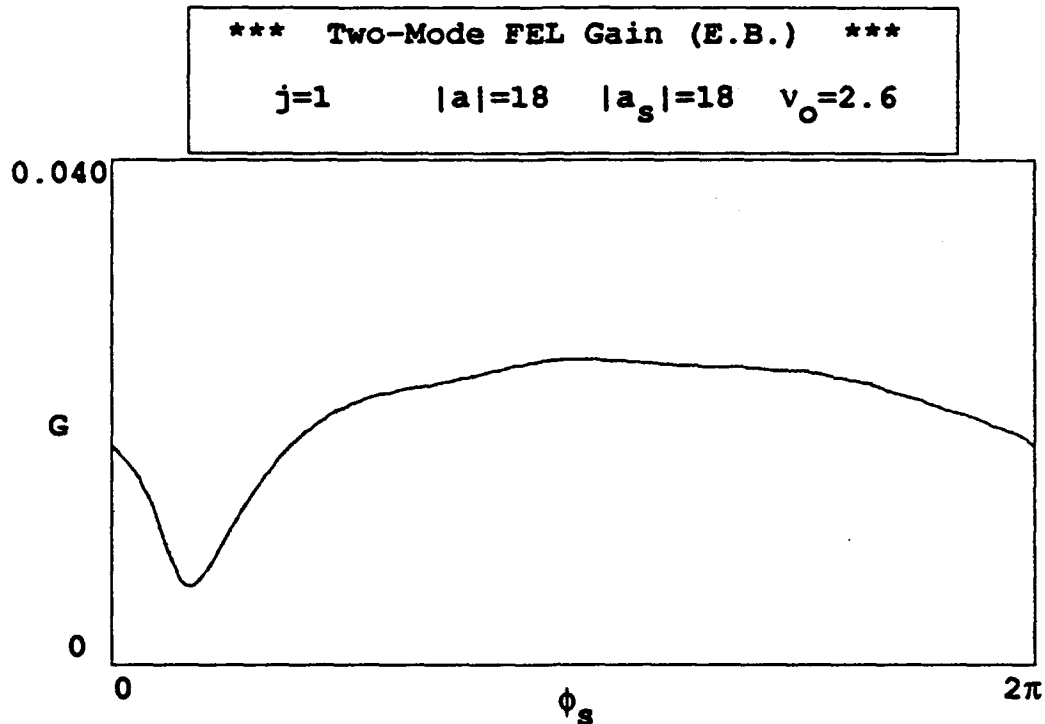


Figure 4-5: Optical field gain vs. initial sideband phase using energy conservation

The gain can also be determined from the two-mode wave equations (4-17), and (4-18). Using these, the two-mode gain can be written as $G = (|a_s(1)|^2 + |a(1)|^2 - |a_s(0)|^2 - |a(0)|^2) / (|a_s(0)|^2 + |a(0)|^2)$. Figure 4-6 is a plot of gain versus initial phase difference between the sideband and fundamental modes using the two-mode wave equations to derive the gain. The input parameters are the same as those used for figure 4-5, and the output gain curve is the exact same. This is reassuring because it validates the two-mode theory against the energy conservation method used to generate figure 4-5. A further check of the two-mode theory is made by comparing the gain curves for the two methods with input

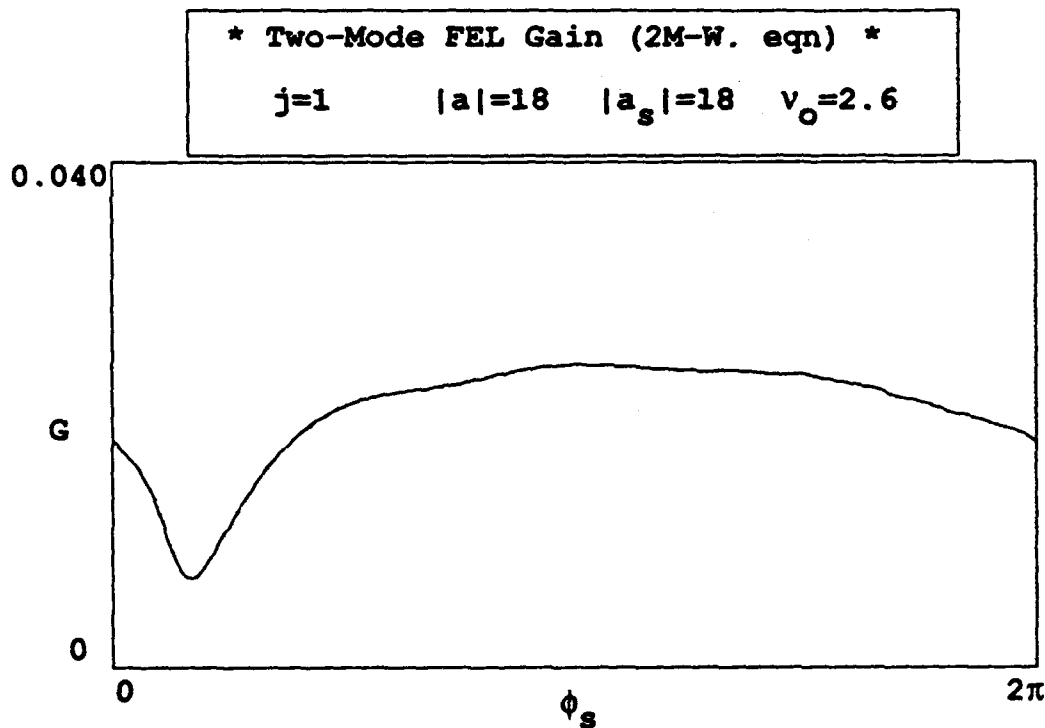


Figure 4-6: Optical field gain vs. initial sideband phase using the two-mode wave equations

parameters of $|a| = 18$, and $|a_s| = 4$. Figure 4-7 plots gain versus phase difference using the energy conservation method, while figure 4-8 plots the same using the two-mode wave equations. The plots are exactly the same illustrating that the two-mode wave equations are valid over a wide range of initial optical field strengths.

Unlike the method of energy conservation using electron phase velocities v , the two-mode wave equation allows the development of each mode to be determined separately. Figure 4-9 plots the gain for each mode separately as a function of initial sideband phase. In the case of this plot, the sideband starts off with the larger gain at $\tau = 0$. Both modes have approximately the same maximum, minimum, and average

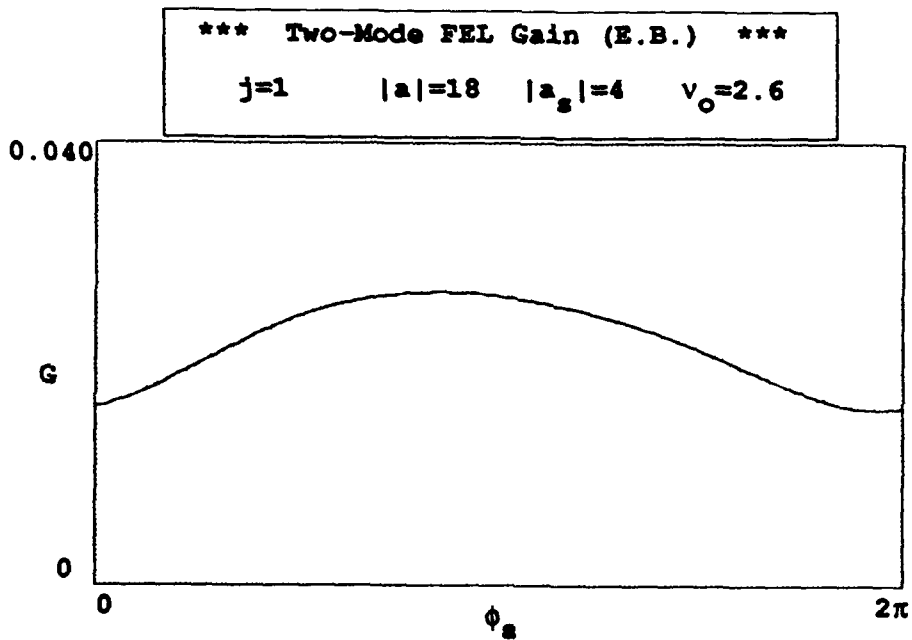


Figure 4-7: Optical field gain vs. initial sideband phase using energy conservation

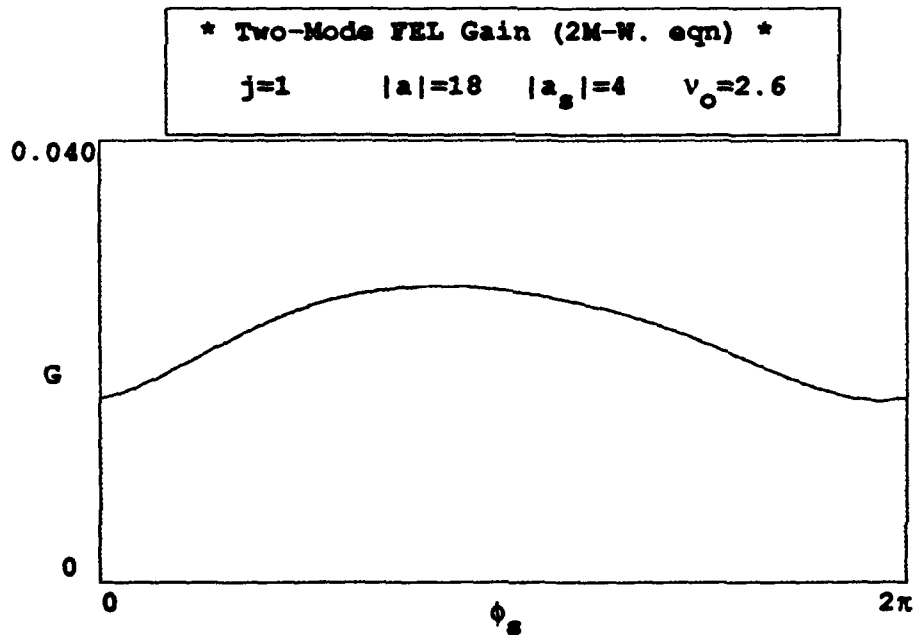


Figure 4-8: Optical field gain vs. initial sideband phase using the two-mode wave equations

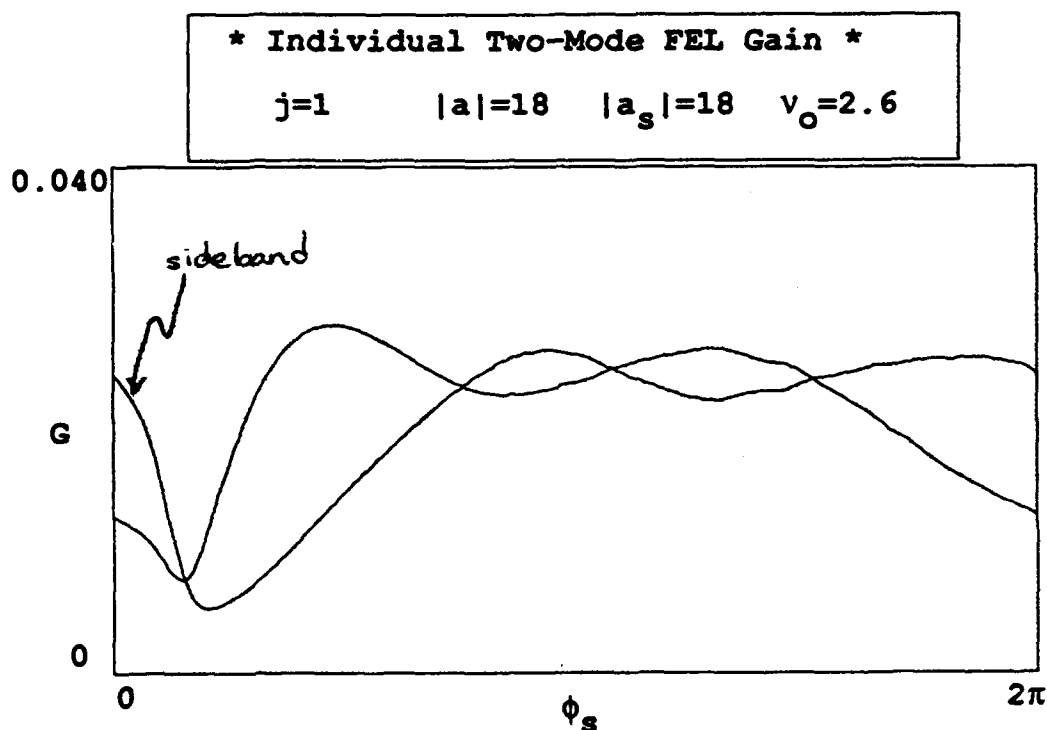


Figure 4-9: Optical field gain for each mode vs. initial sideband phase
using the two-mode wave equations

gains along with some symmetry with respect to each other around the initial sideband phase for minimum gain.

Figure 4-10 plots the individual mode gains with initial optical fields of $|a| = 18$, and $|a_s| = 4$, as in figures 4-7 and 4-8. For this example the sideband gain starts negative at $\phi_s = 0$, but reaches a maximum gain of $G \approx 0.10$ at an initial phase difference of $\phi_s \approx 4.0$. It is to be expected that the sideband has a higher maximum gain than the fundamental, since it starts with an optical field that is further from saturation than the fundamental. What is surprising is that there is a significant band of phases where the sideband gain is negative.

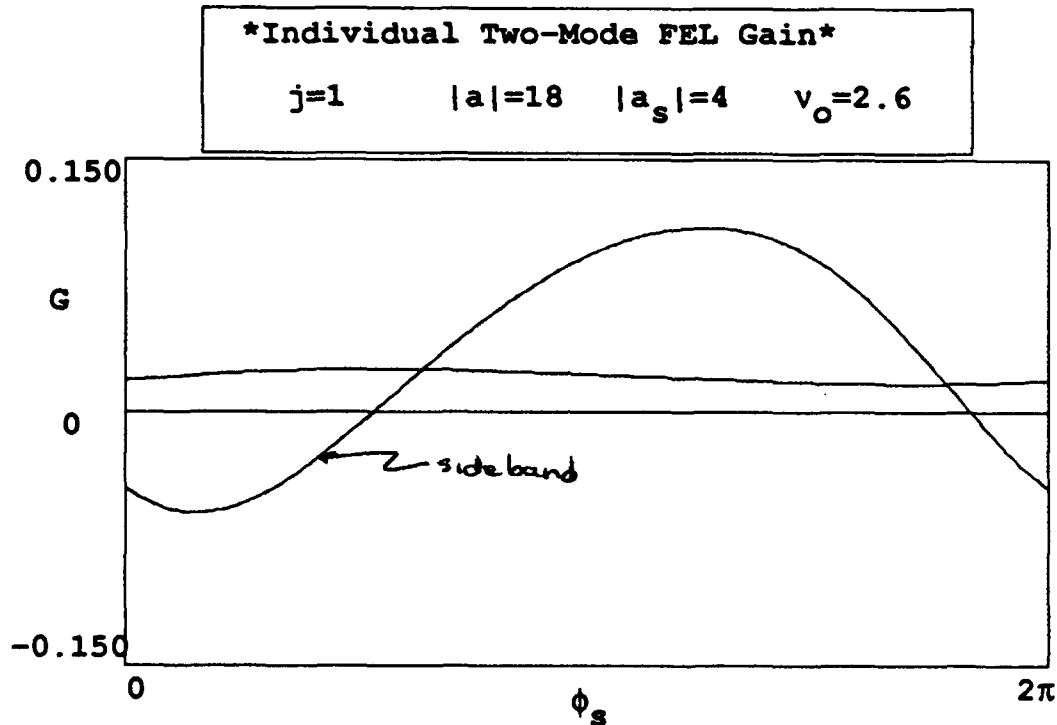


Figure 4-10: Optical field gain for each mode vs. initial sideband phase
using the two-mode wave equations

Just as the gain can be calculated from the two-mode wave equations, so can the phase evolution for each mode, $\Delta\phi$, and $\Delta\phi_s$. The difference between these two phase evolutions determines how much the optical pulse shape slips ahead or behind of reference mark traveling down the undulator with it at the speed of light. For example, a difference between the two phase evolutions of π would mean that if a reference mark was placed by the peak of a two-mode optical wave at the beginning of the undulator, the mark would be at a trough in the optical wave when the wave reached the end of the undulator. What holds for reference marks also holds for electrons, a difference in phase evolutions or phase shift between the two optical modes is equivalent to a phase shift in ζ for an electron interacting with the optical

field. Because of this, large shifts in phase can have a strong influence on electron dynamics and subsequent gain. From simulations it turns out that large differences in the two phase evolutions occur when the amplitude of the sideband is very small compared to the fundamental mode. But at that point, the optical envelope resembles one for a single mode wave and any phase shift of the optical wave from $\tau = 0 \rightarrow 1$ has little effect on the electron dynamics. As the sideband grows to the same order of magnitude as the fundamental the phase shift between modes decreases so its effects can be neglected from $\tau = 0 \rightarrow 1$.

Figure 4-11 plots the phase shift, $\Delta\phi_d$, between sideband and fundamental as a function of the initial sideband phase. The initial optical fields are $|a| = |a_s| = 18$, consistent with previous examples. The maximum phase shift never exceeds 0.03 and the average phase shift is 0.007, both very small numbers relative to a half period phase shift of π . It should be noted that the maximum phase shift occurs at the same approximate initial sideband phase as that for minimum gain shown in figure 4-6. At this phase $\phi_s \approx 0.2\pi$ both modes have minimum gain which corresponds to the maximum phase evolution for each. Because of this the difference in phase evolutions is more significant then at an initial sideband phase where both modes show larger gain.

The above discussion showed with two optical modes present, the importance of the initial sideband phase at $\tau = 0$ with respect to the electrons. The electron dynamics, optical field gain, and optical field phase shift are all dependent on the initial sideband phase. The question then becomes, when looking at the performance of an FEL after one or multiple passes of the optical field with a sideband present, which initial sideband phase if any is controlling or critical to the FEL interaction? The answer appears to be the complete spectrum of sideband phases from $0 \rightarrow 2\pi$. Whether looking at a pulse of length greater then a slippage distance or a continuous wave consisting of two modes, electrons injected into the undulator will be distributed over all possible initial phases of the sideband on each pass. This is because all

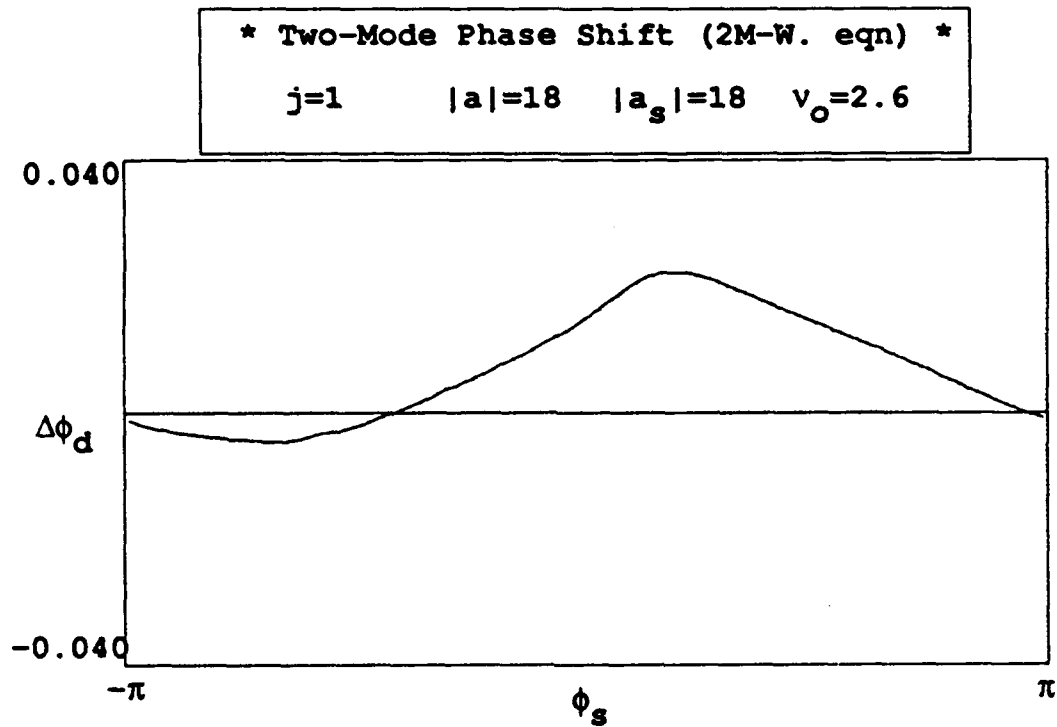


Figure 4-11: Optical field phase shift vs. initial sideband phase using the two-mode wave equations

initial sideband phases are present in one slippage distance of the electron pulse. If figure 4-1 represents the optical wave shape over one slippage distance $N\lambda$, at the beginning of the undulator the incoming electron beam can be pictured uniformly distributed underneath it. Since all initial phase differences of the sideband and fundamental are represented by electrons, to determine the FEL performance at the end of each optical wave pass the gain of each mode and the difference in phase rates should be averaged over all initial sideband phases [Ref. 12].

Figure 4-12 is a simulation over multiple passes that averages the fundamental and sideband gain over the spectrum of initial sideband phases $\Delta\phi_d$ for each pass. The gain for each mode, as well as the resonator loss coefficient Q , is then used to

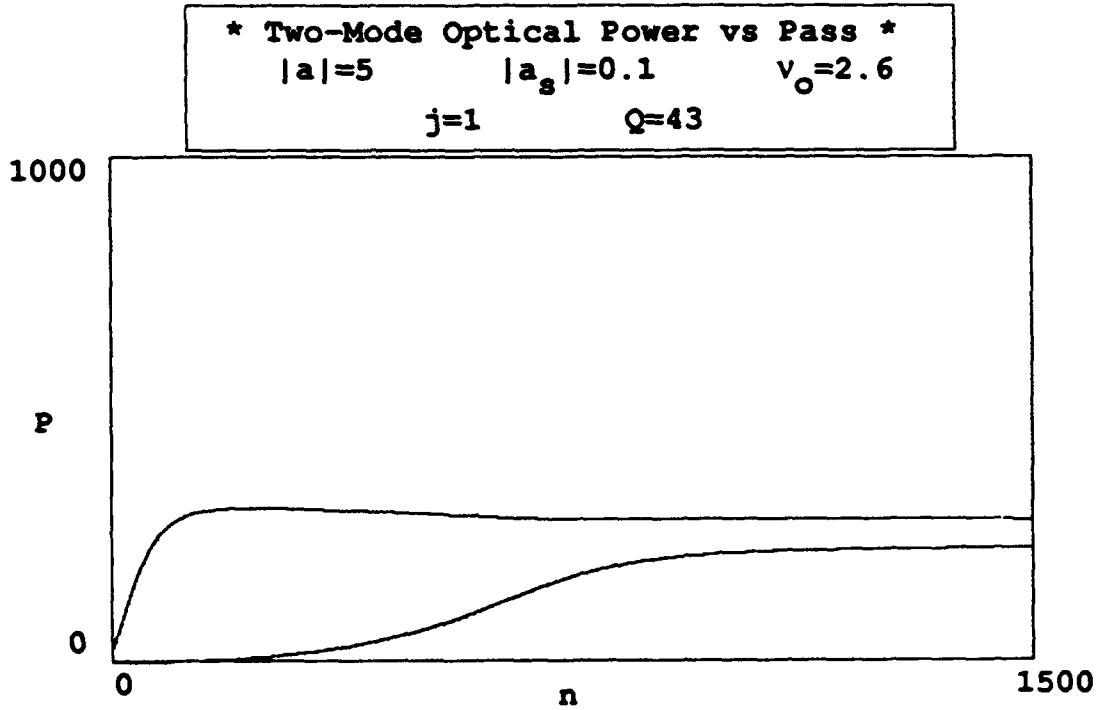


Figure 4-12: Fundamental and sideband power vs. pass number using two-mode wave equations to derive gain for each pass

determine the change of the optical field of each mode for the next pass through the undulator. The horizontal axis of the plot represents the number of passes n through the undulator for the optical waves. The vertical axis represents the power for each mode at the end of a pass, $P = |a|^2$. The initial optical fields are $|a| = 5$, and $|a_s| = 0.1$. These are chosen to be slightly below saturation values so as to minimize simulation run time at low field strengths while still showing the development of the sideband and steady-state values. The dimensionless current density is $j = 1$, the initial phase velocity is $v_0 = 2.6$, and the loss coefficient is $Q = 43$. The simulation is allowed to run over $n = 1500$ passes. The plot shows the fundamental mode quickly reaching saturation in $N \approx 100$ passes, then slightly declining as the sideband slowly

reaches a steady-state value. The sideband development is delayed until the fundamental mode saturates. Then it grows, but at a slower rate, until reaching approximately the same field strength. The combined optical power for the two modes is $P = |a|^2 + |a_s|^2 = 500$. From the plot, it seems clear that the saturation value for the fundamental mode does not appreciably change when a sideband is present.

A comparison is made between the above two-mode simulation and a true multi-mode simulation using identical values of $Q = 43$ and $j = 1$. Figure 4-13 illustrates a multi-mode simulation with an initial optical field of $|a| = 1$, with random signal fluctuations $\delta a = 1$ imposed at the fundamental mode. Over many passes other modes are allowed to evolve at their natural frequency. Periodic boundary conditions are placed on the optical wave two slippage distances in length, with the simple pendulum and wave equations being solved for sample electrons at sites equally spaced along the optical wave. From left to right, the upper three frames show the final optical wave shape, optical spectrum, and electron spectrum at the end of the simulation. The middle three frames, from left to right, show the evolution of the optical wave shape, optical spectrum, and electron spectrum versus the undulator pass number n . The lower three frames, from left to right, display the optical power gain versus n , the small signal gain spectrum, and the optical power versus n . The final optical spectrum shows two distinct modes of equal amplitude separated by $\nu_s = 2\pi$, which is the same as the two-mode simulation. The final optical power, $P = 520$ for the multi-mode simulation, closely matches the two-mode simulation as well. Just as in the two-mode simulation, the lower-right frame of the multi-mode simulation shows the optical power rapidly rising until saturation of the fundamental mode. The power remains constant until the sideband starts to evolve, increasing to a new steady-state level but at a slower rate than the previous growth. The sideband starts development quicker in the two-mode simulation, but this is due to an initial sideband field of $|a_s| = 0.1$ being present to start the simulation vice noise as in the multi-mode simulation.

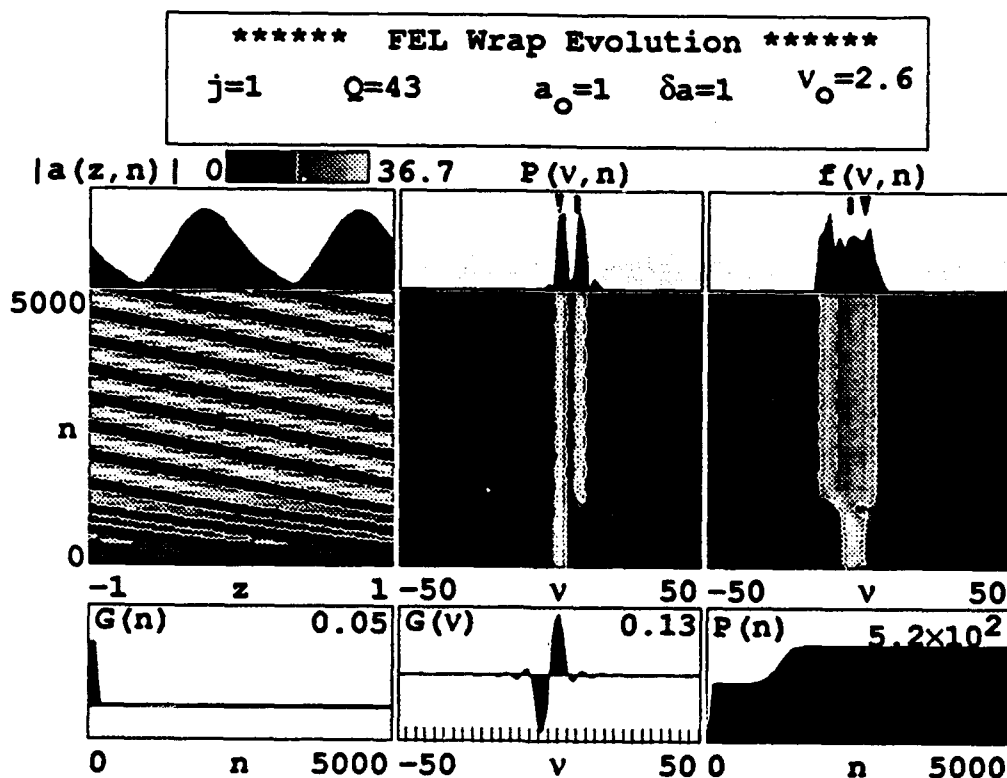


Figure 4-13: Multi-mode simulation showing fundamental and single sideband

The left-upper frame shows the final optical wave shape over two slippage distances. This wave shape corresponds to the optical profile in figure 4-1, but inverted since the wave is overtaking the electrons vice the electrons overtaking the wave. The left-center frame shows how the optical field shifts phase over many passes. The frame is fixed at the end of the undulator and the optical wave is considered to maintain the same phase from the end of one pass to the beginning of the next pass. If there were no phase evolution of the optical field down the undulator the peaks of the optical field would line up at the same position in the frame after each successive pass. The optical wave drawing to the left would indicate a positive phase

shift in the two-mode model with the fundamental phase being held constant at zero. From the multi-mode simulation, the phase shift is $\Delta\phi_d \approx .012$, determined by finding the number of passes it takes the optical field peak to slide one slippage distance (2π radians) and dividing the former into 2π . Figure 4-11 approximately represents the steady-state optical fields of the multi-mode simulation gives a value of $\Delta\phi_d = 0.007$ when averaged over all initial sideband phases. While not exact the two-mode method gives values that account for the magnitude and direction of phase shift experienced by the optical wave in the multi-mode simulation.

F. TWO-MODE SATURATION

For a single mode optical wave, saturation occurs when the optical field strength reaches a level where the electrons initially bunch in phase-space, but then debunch as $\tau \rightarrow 1$. As the electrons debunch they start to increase their phase velocity v , and take away energy from the optical field that they had previously deposited. Figure 4-14 illustrates the phase-space evolution for a single mode optical field of $|a| = 25.4$. This particular amplitude is chosen because it is equal in optical power to the time averaged two mode optical field with $|a| = |a_s| = 18$. The box to the right of the phase-space evolution plots gain as a function of τ . The gain peaks at $\tau \approx 0.75$, and then starts to decrease. This is due to the electrons starting to move to absorption of the optical field and debunch at $\tau \approx 0.75$. From the FELs standpoint maximum gain could be achieved by shortening the undulator by one quarter. It would seem that a shorter undulator is the way to enhanced FEL performance. Unfortunately a shorter undulator would significantly degrade performance prior to saturation. The solution to improved FEL performance would be to design an undulator that could somehow shed a portion of its length just as saturation is reached. While this may be physically impractical, the presense of a sideband accomplishes the same effect.

Figures 4-1 and 4-2 show how an equal magnitude sideband acts to decrease the effective distance of the undulator by decreasing the amount of time an electron

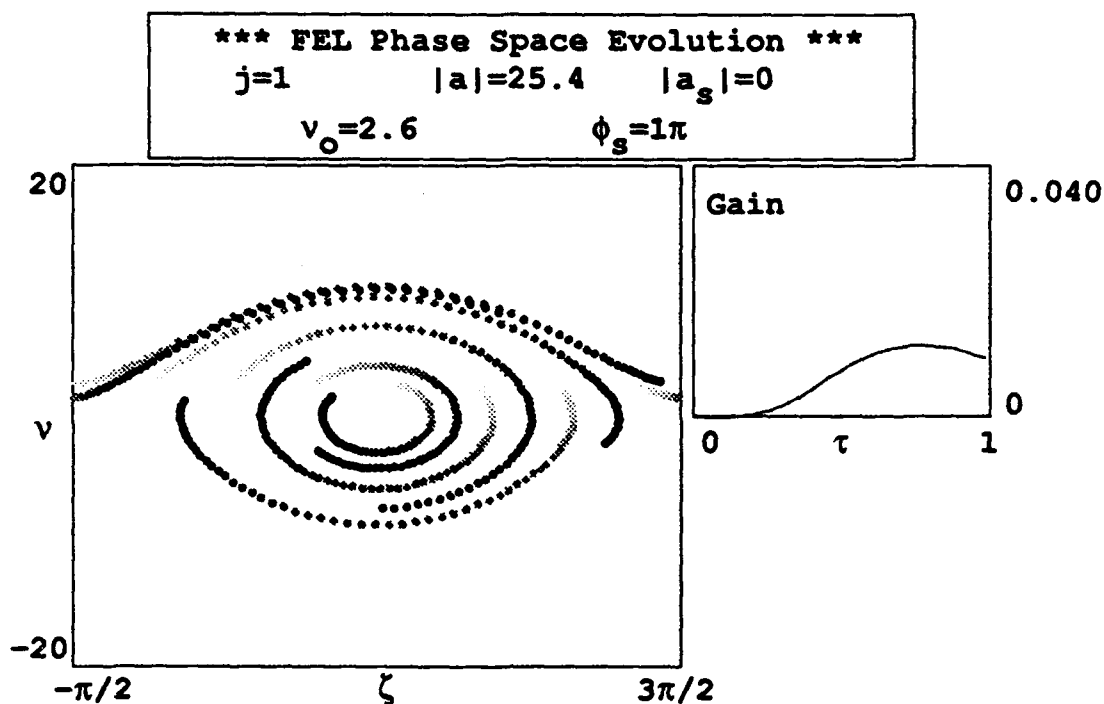


Figure 4-14: Single-mode phase-space with gain vs. τ

sees a significant optical field. Figure 4-15 shows the phase-space evolution and plot of gain versus τ for a two mode optical field with $|a| = |a_s| = 18$ and an initial phase difference of $\phi_s = \pi$. Underneath these plots is a plot of the gain spectrum from figure 4-5 with a vertical line depicting where the phase-space plot belongs relative to the initial sideband phases possible. For the gain versus τ plot the curve levels out at a value at least double that for figure 4-14, and it does not decrease after reaching its peak. The phase-space evolution shows the electrons going into open orbits with $v < 0$ vice closed synchrotron orbits as in figure 4-14 that rob energy from the optical wave. In addition, the electrons appear to stay bunched around $\zeta = \pi$, leading to a larger peak gain. Of course figure 4-15 is the phase-space evolution for only one initial sideband phase, the one that gives maximum gain. Figures 4-16 and 4-17 show

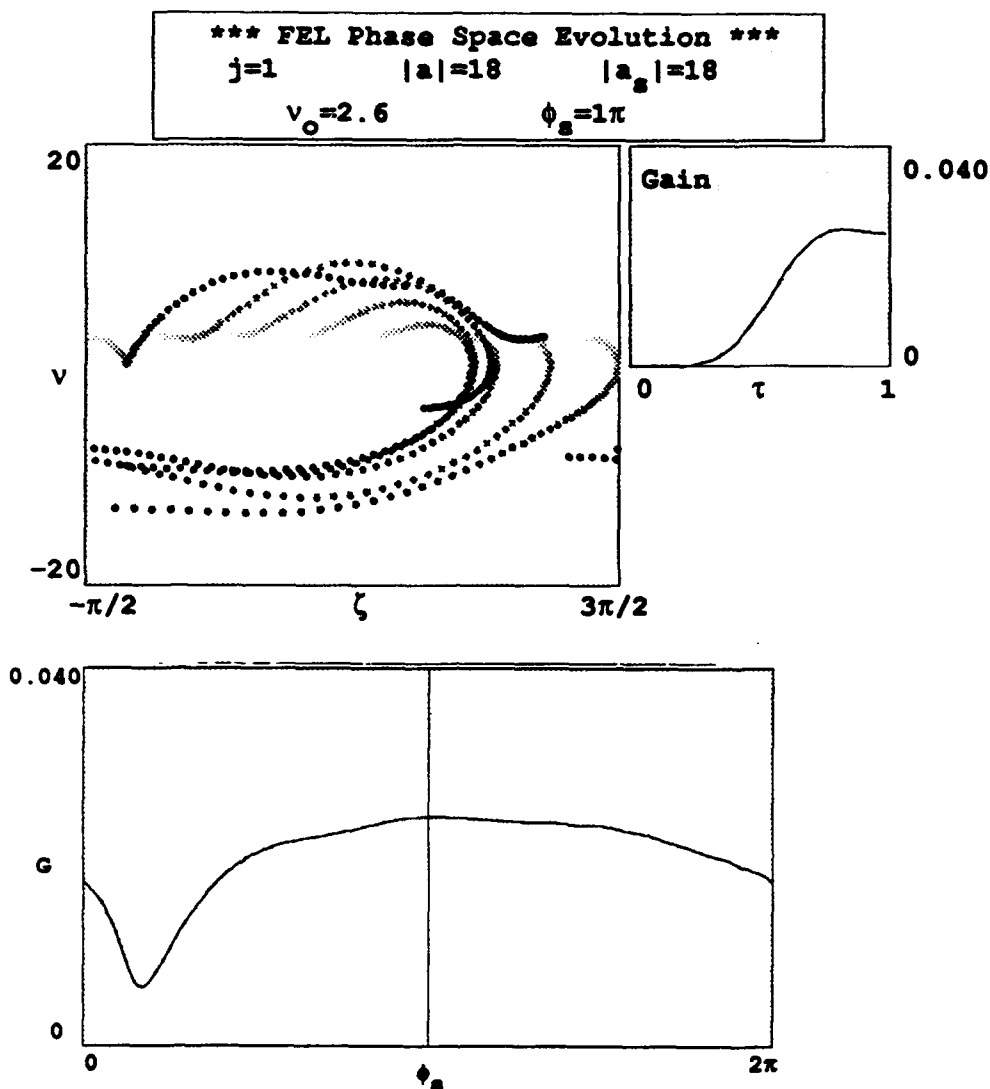


Figure 4-15: Two-mode phase-space with gain vs. τ , $\phi_s = \pi$

the phase-space and gain evolutions for initial sideband phases of 0.4π and 1.6π respectively. In both cases, the final gain at $\tau = 1$ is greater than for the single mode of figure 4-14 even though the optical waves have equal power. What should be noted in both phase-space plots is some synchrotron motion of the electrons causing a dip or plateau in the gain prior to $\tau = 1$. It appears that the initial sideband phases that do not contribute as much to the gain as the phase with maximum gain are critical in

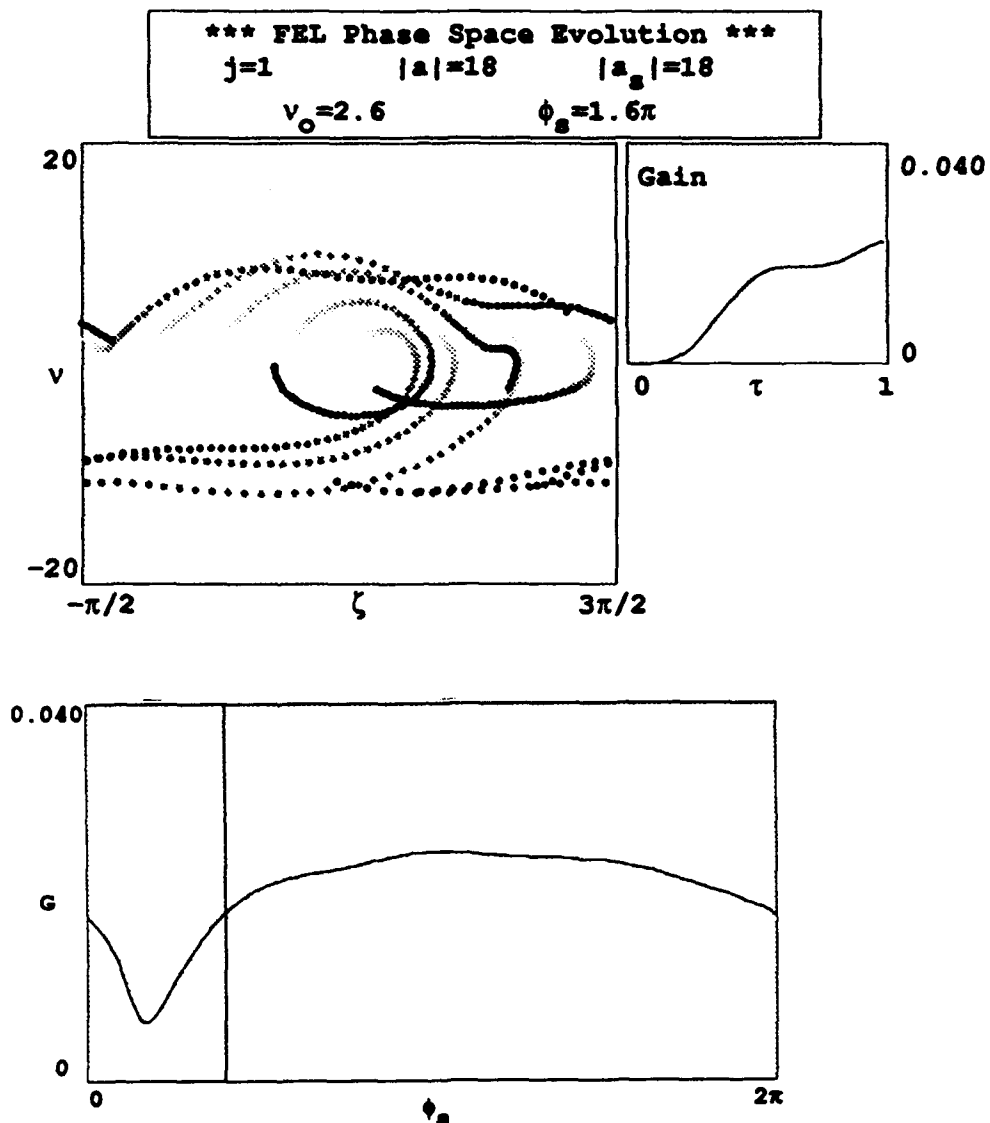


Figure 4-16: Two-mode phase-space with gain vs. τ , $\phi_s = 0.4\pi$

maintaining the sideband present with electron synchrotron motion that can be amplified over one or many passes.

Increasing the gain over each pass for the optical wave leads to increased power. As the power increases with each pass the gain will start to decrease until the gain from each pass is equal to the losses from the resonator cavity. When this

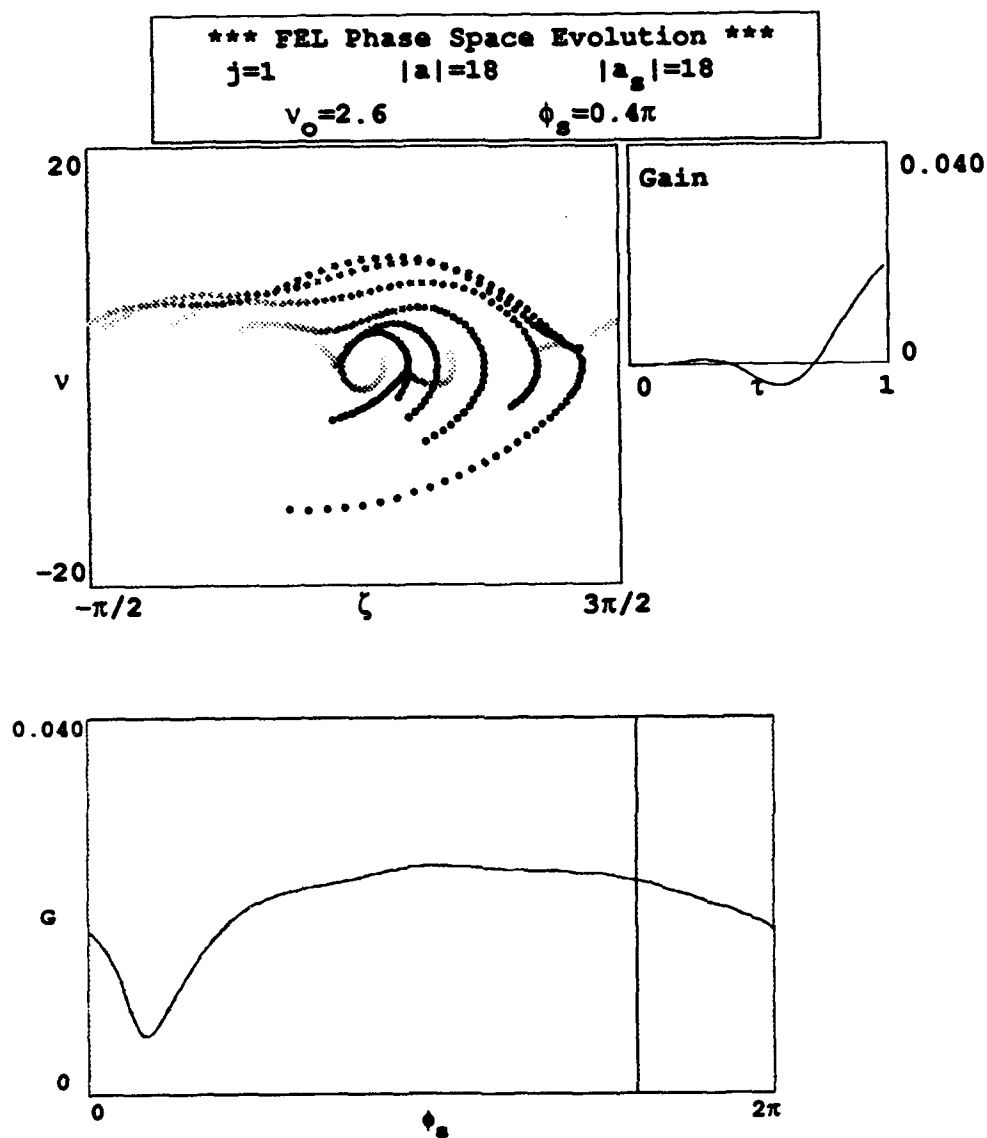


Figure 4-17: Two-mode phase-space with gain vs. τ , $\phi_s = 1.6\pi$

occurs, steady-state is achieved. With a sideband present, the larger gain allowed prior to saturation as compared to the single-mode optical field, produces larger power at steady-state operation.

G. CONCLUSION

With a single sideband of the approximately the same amplitude, offset by $\nu_s = 2\pi$ from the fundamental mode, the two modes combine to form a beat wave that oscillates one half a period as seen by a relativistic electron traveling down the undulator. The electron phase-space paths are best understood in terms of this beating optical field. It can be thought to cause an "instantaneous separatrix" that expands and contracts with the optical field amplitude. The initial phase of this optical field, determined by the initial sideband phase is critical to the electron dynamics and subsequent optical field evolution. Both the gain and phase rate of the optical field are dependent on the initial sideband phase.

Comparing gain curves calculated using energy conservation and the two-mode wave equation, one finds that they are exactly the same over a wide range of amplitudes. In addition, the two-mode wave equations allow the gain for each mode to be separated and analyzed, unlike energy conservation techniques. When both modes are of approximately equal amplitude, the maximum gain is achieved when the initial sideband phase is π . Because an incoming electron beam will evenly distribute electrons over all initial phases, the gain and phase rate must be averaged over all initial sideband phases.

With a steady-state sideband present, the length of the undulator is effectively shortened and allows more gain than when only a single mode is present. Hence, a multi-mode optical field can postpone the onset of saturation, allowing the FEL to generate more power than a single mode.

LIST OF REFERENCES

1. J. M. J. Madey, J. Appl. Physics. **42**, 1906 (1971).
2. L. R. Elias, W. M. Fairbank, J. M. J. Madey, G. J. Schwettman, T. I. Smith, Phys. Rev. Lett. **36**, 717 (1976).
3. D. A. G. Deacon, L. R. Elias, J. M. J. Madey, G. J. Ramian, H. A. Schwettman and T.I. Smith, Phys. Rev. Lett. **38**, 892 (1977).
4. W. B. Colson, "Classical Free Electron Laser Theory", Chapter 5 in "*Free Electron Laser Handbook*", W. B. Colson, C. Pellegrini and A. Renieri (*editors*), North-Holland Physics, Elsevier Science Publishing Co. Inc., The Netherlands (1990).
5. J. D. Jackson, *Classical Electrodynamics*, Wiley, New York, (1975).
6. R. Rohatgi, H. A. Schwettman, T. I. Smith, and R. L. Swent, Nucl. Instr. and Meth. **A272** (1988) 32-36 (Proc. 9th Int. FEL Conf. 1987).
7. W. B. Colson and S. K. Ride, Phys. Lett. **A 76**, 379 (1980).
8. S. Benson and J. M. Madey, *Free Electron Generators of Coherent Radiation*, eds. C. A. Brau, S. F. Jacobs and M. O. Scully, SPIE **453**, 55 (1983).
9. J. C. Frisch, *Time Dependent Measurements on the Superconducting Accelerator Free Electron Laser*, Ph.D. Dissertation, Stanford University, (1990).
10. W. B. Colson, Nucl. Instr. and Meth. **A250** (1986)168-175 (Proc. 7th Int. FEL Conf. 1985).
11. D. H. Kiel, *Two Nonlinear Models of the Free Electron Laser*, Master's Thesis, Naval Postgraduate School, (1990).
12. N. M. Kroll and M. N. Rosenbluth, *Physics of Quantum Electronics*, Vol. **7**, 147 (1980).

INITIAL DISTRIBUTION LIST

- | | | |
|----|--|---|
| 1. | Defense Technical Information Center | 2 |
| | Cameron Station | |
| | Alexandria, Virginia 22304-6145 | |
| 2. | Library, Code 52 | 2 |
| | Naval Postgraduate School | |
| | Monterey, California 93943-5002 | |
| 3. | Professor William B. Colson, Code PH/Cw | 9 |
| | Department of Physics | |
| | Naval Postgraduate School | |
| | Monterey, California 93943-5000 | |
| 4. | Professor John R. Neighbours, Code PH/Nb | 1 |
| | Department of Physics | |
| | Naval Postgraduate School | |
| | Monterey, California 93943-5000 | |
| 5. | Professor K. E. Woehler Code PH/Wh | 1 |
| | Chairman, Department of Physics | |
| | Naval Postgraduate School | |
| | Monterey, California 93943-5000 | |